Design and Prototyping of a Low-Speed Flywheel System for Automotive Brake Energy Recovery

Undergraduate Honors Thesis

Presented in Partial Fulfillment of the Requirements for

Graduation with Distinction

at The Ohio State University

By

Sheng Xu

* * * * *

The Ohio State University

2012

Defense Committee:

Professor Marcello Canova, Advisor

Professor Yann Guezennec

Abstract

Fossil fuels are an important energy source in transportation. Since fossil fuels are non-renewable resources which will exhaust sometime, the need for energy-efficient vehicles with energy recovery systems has become a necessity to optimize the utilization of fossil fuels in transportation. Currently, great interest is being devoted to research sustainable transportation, combining highly efficient vehicles with various forms of energy storage and recovery. This thesis investigates a mechanical flywheel energy recovery system for hybrid vehicle applications, which has become the subject of extensive research as an alternative to electrochemical batteries for on-board energy storage. The objectives of the research are to design a prototype of a low-speed flywheel system and integrate the hardware of the control systems to demonstrate the automotive brake energy recovery process. As a part of a large project conducted at the Ohio State University, the prototype is used to further investigate control algorithms to improve the efficiency of the flywheel-based energy recovery system.

Acknowledgements

I would like to thank my advisor Professor Marcello Canova for giving me the opportunity and the guidance of the undergraduate honor research project. I also would like to thank Dr. Fabio Chiara for his help and direction in the whole period of research. Then I would like to thank Dr. Codrin-Gruie Cantemir for teaching the design concepts to me. I also want to thank the other member involving the flywheel project, Joshua McDonough and Kingsly Jebakumar, for their prior work and helps. Additional, I would like to thank Prof. Yann Guezennec and Prof. Robert Siston for teaching me the presentation skills in ME H783 courses.

Table of Contents

Page

List of Figures

Figure **Page**

List of Tables

Table **Page**

Chapter 1: Introduction

1.1 Motivation

For many years, fossil fuels are consumed as a primary energy source in transportation and industry. Currently, the United States consumes 19.6 million barrels of oil per day, which is more than 25% of the world's total production [1]. Despite predictions that the U.S. will exhaust its supply of oil in forty years, the demand is on the increase, and is predicted to continue increasing, because of the ever increasing population and demand for mobility[1]. The increasing demand of fuel to meet these needs inevitably causes a rising of oil price. Figure 1 below shows the fluctuation of the average fuel price of the pump from 2004 to present in Columbus, OH. The average retail price raised more than 120% from March 2004 to March 2012.

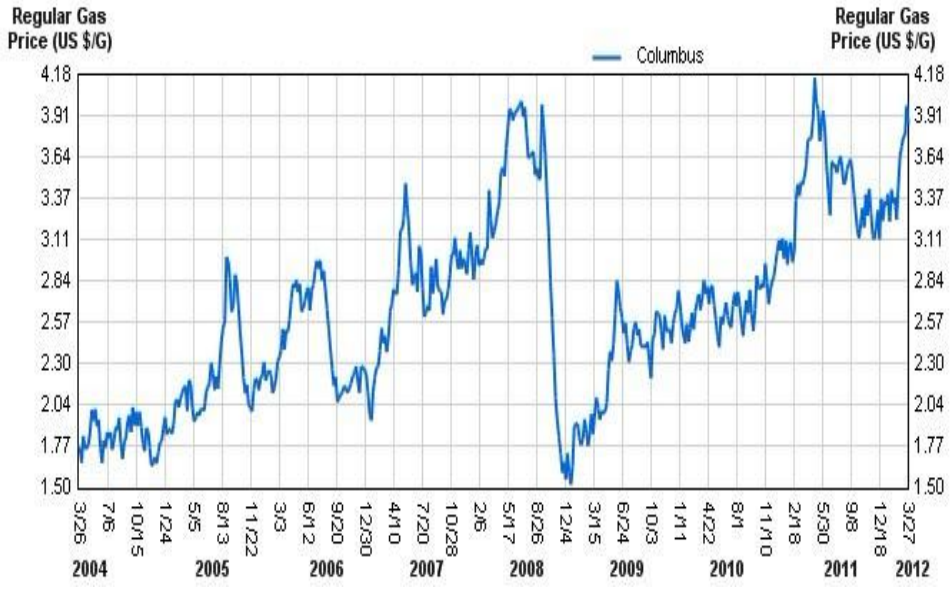

Figure 1: Average Regular Gasoline Retail Price in Columbus, OH from 2004 to 2012 [2]

This issue is increasing awareness about the energy crisis of the non-renewable fossil fuel resource. To moderate the potential crisis, the need for sustainable development has become a necessity, especially in the area of the transportation. The Energy flow chart (Figure 2) shows the relative size of primary energy resources and end use in the United States, with fuels compared on a common energy unit basis.

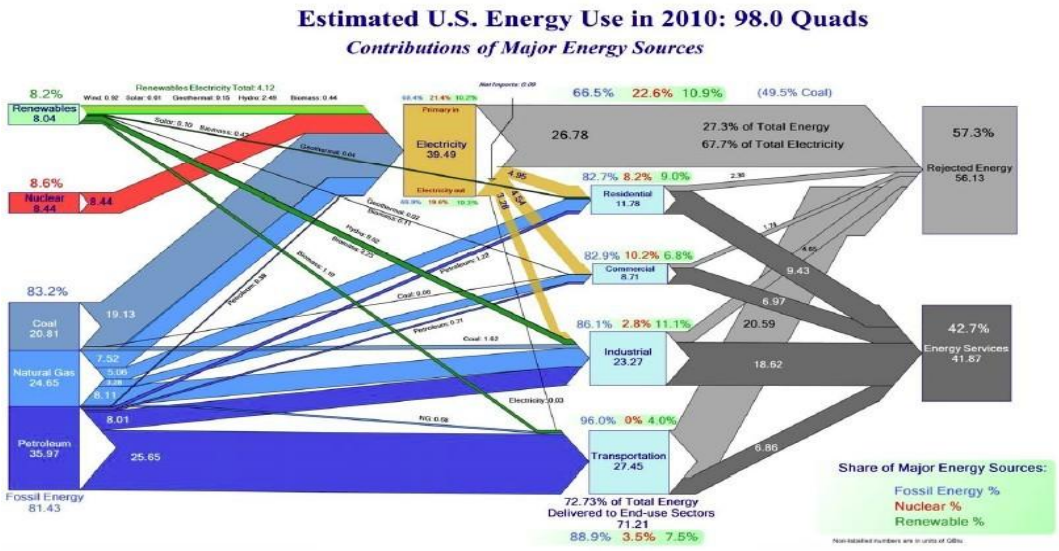

Figure 2: Estimated US Energy Use in 2010 by Source & Sector [3]

The significant amount of rejected energy, which refers to energy that is lost in conversion processes, is observed in the transportation sector. The total energy consumed was around 27.5 Quad Btu of which ~20.6 Quad Btu was rejected energy [3]. This huge inefficiency in energy conversion in the transportation sector has called for developing technical solutions towards sustainable transportation, normally combining highly efficient vehicles with alternative energy resources.

1.2 Analysis of Kinetic Energy Recovery

To move a vehicle on the road with a variable speed profile, the variation in kinetic energy of the vehicle should overcome the energy losses due to the aerodynamic friction, the rolling resistance and the energy dissipation in the brakes. Unfortunately, the energy losses to the aerodynamic friction and the tire rolling friction are non-recoverable. However, one possible method to improve fuel economy is to a part of the vehicle kinetic energy that would otherwise be dissipated to the brakes during deceleration, store it and utilize it to accelerate the vehicle later. This process of recovering the energy dissipated to the brakes is defined as "regenerative braking". Hybrid vehicles can recover braking energy to increase vehicle efficiency.

There are several methods developed to adopt regenerative braking for vehicle use. One method involves using an electric generator to convert the braking energy into electrical energy and store it in a chemical battery. The stored energy is then released to accelerate the vehicle when needed, by using the electric machine as a motor. Alternatively, energy can also be stored mechanically using a rotating disc (flywheel) with appropriate inertia, as well as a power transmission system. In order to store energy, the flywheel speed should be increasing while the vehicle speed is decreasing. Vice versa, the flywheel must decelerate while the vehicle speed is increasing to release the energy.

Though a regenerative braking system plays a role in the vehicle's braking, it cannot completely replace friction brakes for the safety reasons. In cases of potential energy storage system failure or desired deceleration beyond the capability of the regenerative system, friction brakes must still be capable of providing sufficient stopping capability [4].

1.3 Overview of Hybrid Electric Vehicles (HEVs)

HEVs provide an option of sustainable transportation to improve fuel efficiency and moderate the fuel energy crisis. HEVs use electric machines to convert the braking energy into electrical energy and store it in a chemical battery. The electric machine behaves as a generator and charges the battery by drawing regenerative braking energy. When acceleration is commanded by the HEV, the electric machine behaves as a motor and provides torque at the expense of stored energy.

Currently, HEVs are the most common hybrid vehicles that car companies produce in the market. The first widely available electric hybrid vehicle was the Toyota Prius released in Japan in 1997. Initially hybrid vehicles were considered unnecessary because of the low cost of fuels, but the continuously increasing oil price in the world forced more and more automakers to pay attention to hybrid vehicles after 2000. Statistics showed that worldwide sales of hybrid vehicles produced by Toyota, the market leader, have topped the 3-million mark, with more than 3.03 million units sold worldwide as of 28 February 2011 since sales began in 1997 [5]. Figure 3 below indicates the obviously increasing trend of the Toyota hybrid sales.

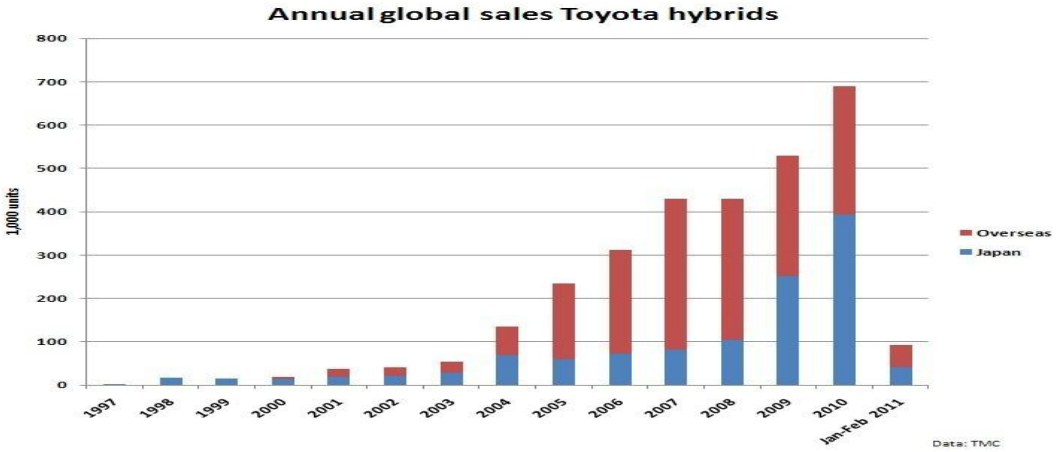

Figure 3: Annual Toyota Hybrid Sales from 1997 to Feb 2011 [5]

1.4 Alternative Energy Storage Systems (AESS) for Hybrid Vehicles

Besides the rapid development of the HEVs, great interest is being devoted today to study the devices to store energy in the other forms. The alternative energy storage systems (AESS) may offer interesting opportunities for the feasibility of low-cost hybrid powertrains. Figure 4 shows the specific power and specific energy for some short-term energy storage systems. Flywheels usually have higher specific power than batteries. In addition, flywheel systems have the advantage of relatively little performance degradation over time regardless of the depth of discharge in terms of energy storage capacity [6].

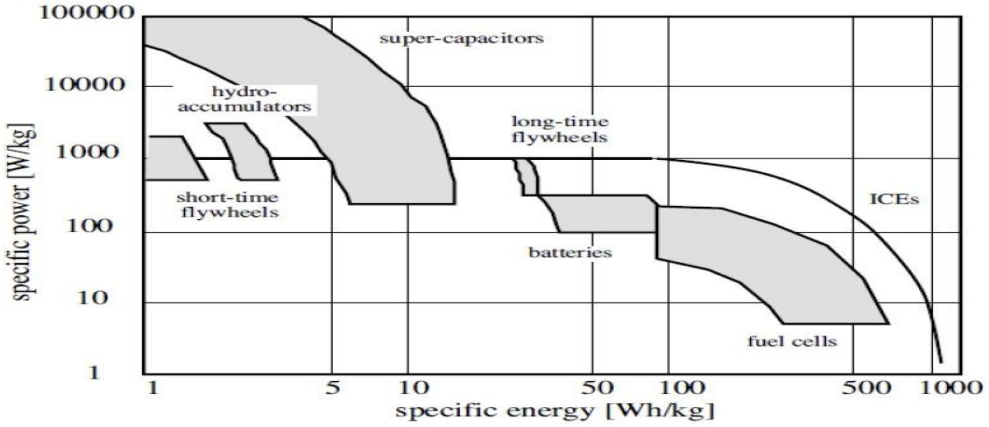

Figure 4: Specific Power versus Specific Energy for Energy Storage Systems [6]

The principle of flywheel hybrid vehicles is to store energy in kinetic form. In some applications, flywheel is sealed inside a vacuum container to reduce the friction losses due to the presence of air. The amount of the kinetic energy stored in a flywheel is represented as the formula:

$$E_k = \frac{1}{2} I \omega^2 \qquad (1.1)$$

where E_k is the stored kinetic energy, I is the mass moment of inertia and ω is its angular speed.

The concept of a flywheel energy storage system is relatively simple. A Continuously Variable Transmission (CVT) plays an important role to transfer the energy between flywheel and vehicle. When a flywheel hybrid vehicle is braking, kinetic energy of the vehicle is stored in the flywheel by changing the CVT ratio to force higher flywheel speeds in a way that matches the decreasing vehicle velocity. This way, the flywheel works as a brake to reduce the vehicle speed while storing kinetic energy to increase its own

rotational speed. When the vehicle is commanded to accelerate, the stored energy will return to the vehicle by changing back the CVT ratio to force a lower flywheel speed. Figure 5 below demonstrates a simple flow of energy between flywheel and vehicle.

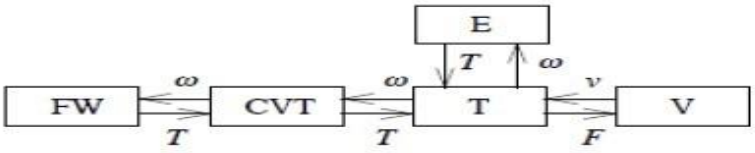

Figure 5: Flow of Power for Flywheel Energy Storage System

where FW is flywheel, CVT is continuously variable transmission, T is transmission, E is engine and V is vehicle drivetrain.

Flywheel can be fabricated with different materials based on the maximum rotational speed and other design constraints. High speed flywheels for speeds above 30000rpm, are usually composed of high strength carbon fiber. A large mass is not desired for high speed flywheels because extra mass means more energy will be needed to accelerate the vehicle. On the other hand, low speed flywheels with speed values below 20000rpm, are generally made of steel or other metals for low cost.

Flywheel systems have been adopted for many areas. For the 2009 racing season, the Federation Internationale de l'Automobile (FIA) has authorized hybrid drivetrains for Formula 1 racing with the clear objective of developing hybrid technology for the use in motorsport. With a focus on safety, the FIA has specified a limit on both the power rating of

the flywheel system at 60kW and the quantity of energy transfer per lap at 400kJ, which provides significant benefits when applied to the racing cars.

1.5 Work Description

The objective of the research is to design a prototype of a low-speed flywheel system to demonstrate the braking energy recovery process that typically occurs in automotive hybrid systems. First a literature review is conducted to understand how the flywheel system operates. Prior work is also important to be studied, in order to obtain the design parameters and specifications. The design of the flywheel system components is implemented using the computer software CATIA to determine the right dimensions. After the computer-based design process, each mechanical component is either ordered or fabricated from material. Then all the mechanical components are assembled, and integrated with a control system, which manipulates the torque transfer in the flywheel system. MATLAB is used to collect and analyze the data for the control system. After testing the assembled system, a basic analysis of the energy transfer dynamics between flywheel and vehicle inertia is demonstrated.

Chapter 2: State of the Arts

In this chapter, the literature sources that are relevant to flywheel design will be reviewed to give insights before the actual design of the Alternative Energy Storage System (AESS) takes place. Prior work conducted at Center for Automotive Research (CAR) of the Ohio State University is recognized as the basis for the preliminary design.

2.1 Comparison between Mechanical Hybrid Vehicles

The paper written by Andrew Barr and Alireza Veshagh [1] provides an overview of a mechanical hybrid project created by the University of Warwick, which is to assess the pneumatic, hydraulic and flywheel hybrid systems as alternatives to electric hybrid system. This paper develops a simulation tool to investigate and evaluate each mechanical alternative to electric hybrid vehicle, and conducts a cost benefit analysis of the different systems from two case studies: 2.6 ton SUV and 17 ton bus applications.

The paper provides configurations of different hybrid systems including series and parallel flywheel hybrids, which may be helpful in the design of flywheel. Figure 6 shows a schematic of the series flywheel hybrid system.

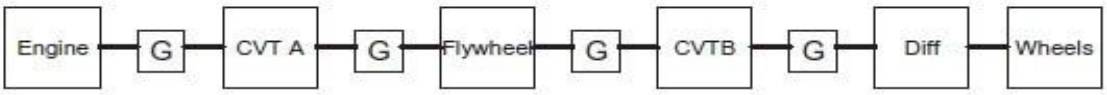

Figure 6: Schematic of Series Flywheel Hybrid System [7]

where G is gear, CVT is continuously variable transmission and Diff is differential. In the series flywheel hybrid system, the engine is connected via a CVT to a flywheel which in turn is connected via another CVT to the wheels [7]. However, the parallel configuration shown in Figure 7 below is similar to the conventional powertrain with the addition of a CVT connected to the system between the engine and the gearbox. The CVT is connected to the flywheel and can control the rate of transfer energy between the flywheel and the vehicle.

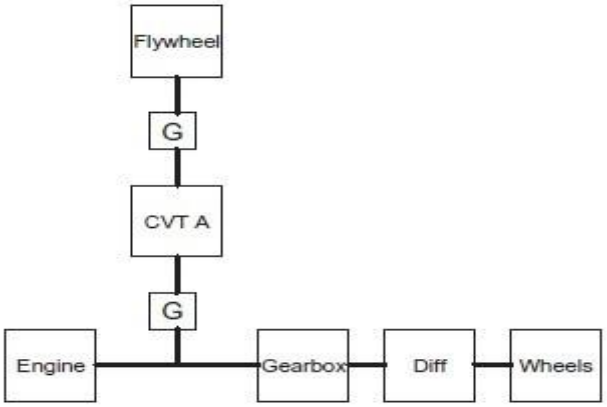

Figure 7: Schematic of Parallel Flywheel Hybrid System [7]

Finally the paper provides an overview of an innovative transmission concept: the flywheel and infinitely variable transmission (FIVT) which combines a flywheel energy system with an infinitely variable transmission shown in Figure 7.

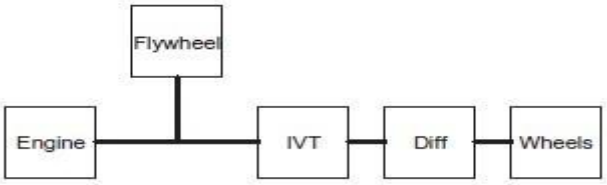

Figure 8: Schematic of FIVT System [7]

The simulated results showed that all hybrid systems have a significant fuel economy benefit compared to conventional vehicles. Electric, flywheel and FIVT systems have the greatest benefit. Pneumatic systems have the least benefit. The bus, driving a typical bus cycle, had a much greater fuel economy improvement than the SUV. The FIVT hybrid is an innovative system which has better fuel economy than other hybrid systems; it is relatively cheap and is selected as the best hybrid system for the project.

The simulated results were consistent within one percent for a SUV comparing with the real world data for the same drive cycle. This is a very good level of accuracy for the simulation. The paper provides configurations of different hybrid systems including series and parallel flywheel hybrids, which may be helpful in the design of flywheel. It also introduces the schematic of the FIVT which can replace CVT and gearbox. This innovation provides an alternative in the designing of CVT. The imperfection in this paper is that it does not provide the controlling algorithm for any of the flywheel system including the FIVT.

2.2 Torotrak

The paper written by Chris Brockbank & Chris Greenwood [2] represents the flywheel-based mechanical hybrid system comprising a high speed composite flywheel and full-toroidal traction drives CVT. The schematic of the full-toroidal variator is provided in Figure 9 to explain the working processes of the CVT.

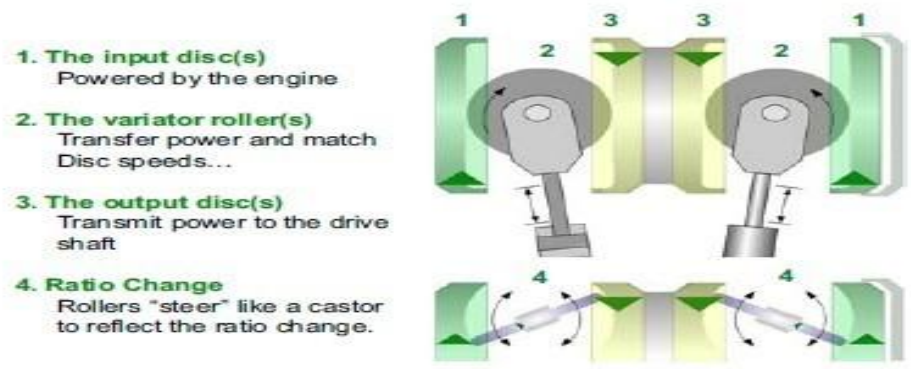

Figure 9: Full-toroidal Variator Schematic [8]

The conventional Torotrak full-toroidal variator comprises four toroidally shaped metal discs which create two toroidal cavities. Each toroidal cavity contains three rollers that transmit power from the input discs to the output discs. The speed ratio of the variator is dependent upon the angle of the rollers within the toroidal cavities.

Simulations of applying the flywheel hybrid to a City Bus are performed. The engine torque profile with and without flywheel shown in the Figure 10 below is obtained to compute the energy saving of the flywheel system. The simulated results show that the energy requirements from the engine reduce from the previous 41.27MJ to 26.36MJ, which is corresponding to a total energy saving of 36.14% or a fuel saving of 33.95%.

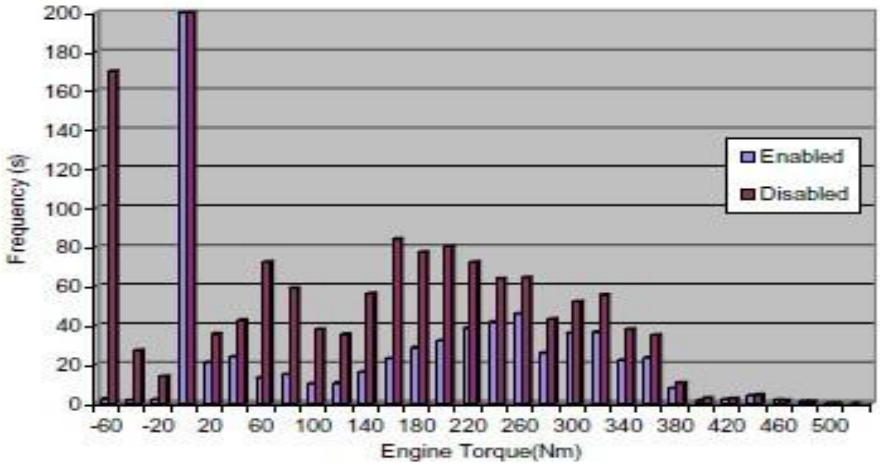

Figure 10: Engine Torque Profile Comparison [8]

This paper introduces an innovative full-toroidal traction drive CVT which control the flywheel system though changing the inclination of the variator. It may be helpful to provide an option in the design of the CVT. However, the detailed steps of computing the energy savings through the engine torque profile are not provided.

2.3 Flybrid

There are many companies that are seriously considering flywheel hybrids as potential alternative for electric hybrids and starting to explore the possibility of commercialization by building prototypes. Flybrid is one of the first companies to reveal the commercialized flywheel systems. The Flybrid Kinetic Energy Recovery System shown in the Figure 11 was a small and light device designed to meet the FIA regulations for the 2009 Formula One season. The key system features were:

- A flywheel made of steel and carbon fibre that rotated at over 60,000 RPM inside an evacuated chamber
- The flywheel was connected to the transmission of the car on the output side of the gearbox via several fixed ratios, a clutch and the CVT
- 60 kW power transmission in either storage or recovery
- 400 kJ of usable storage (after accounting for internal losses)
- A total system weight of 25 kg
- A total packaging volume of 13 litres [9]

The layout of the device was tailored exactly to meet the customer's requirement resulting in a truly bespoke solution that fitted within the tight packaging constraints of a F1 car.

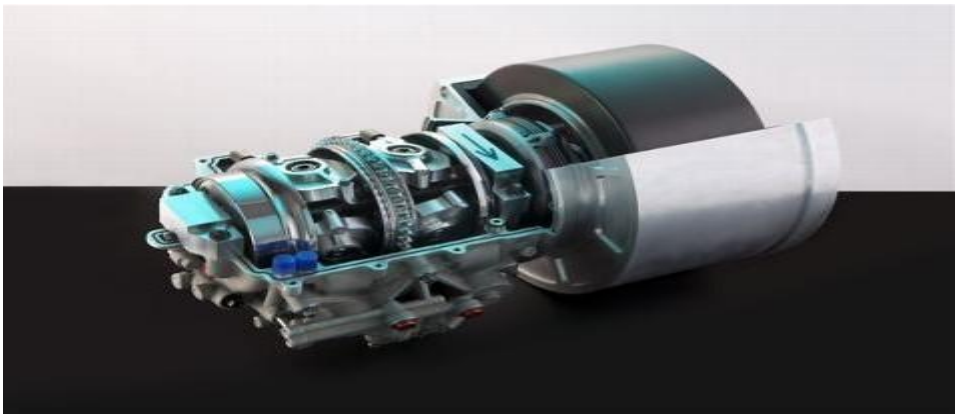

Figure 11: Original CVT Based Formula One KERS [9]

2.4 Prior Work

There has been extensive research in the field of the design of flywheel systems at CAR. The design considered is based on a parallel configuration, where the mechanical ESS

is located between the transmission and the drive axle, as shown in Figure 12 below. This configuration allows for minimal changes in vehicle design and allows for standard drivetrain components to be used [10].

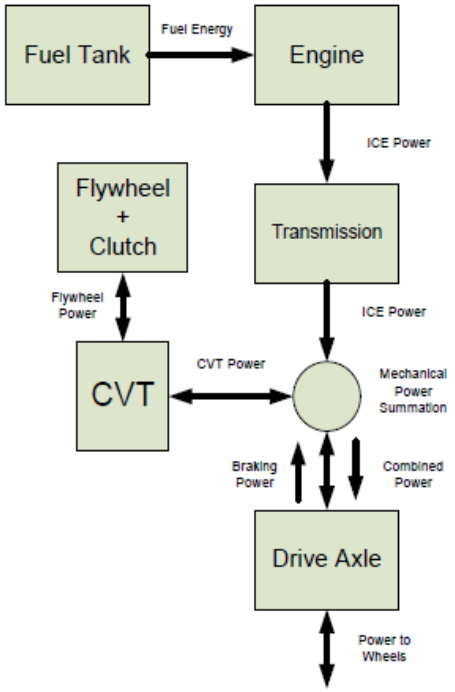

Figure 12: Mechanical Hybrid Powertrain Layout [10]

Once the configuration is finalized, the models are crucial to evaluate the relative performance of designs when the design parameters within the models are altered. The model adopted for the study is based on mid-size SUV parallel hybrid vehicle configuration with the parameters shown in the Table 1.

Table 1: Vehicle Model Details of 2009 Saturn VUE [10]

Weight:	1680kg (base)
Engine:	3.5L V6 LZ4
Transmission:	6 speed automatic
Gear ratios:	4.48; 2.87; 1.84; 1.41; 1; 0.74
Final drive ratio:	2.77
Tire Size:	0.713m diameter (235/60/R17)
Frontal Area:	2.64 m^2

The design of the flywheel system is based on statistical analysis of a synthesized cycle of actual driving data and weightings that favored maximum capture and return of braking energy are used. The statistics obtained is shown in the Table 2 below.

Table 2: Relevant Drive Cycle Statistics for 2009 Saturn VUE on Synthetic Cycle [10]

	Maximum Values	Mean Values	Weighted Mean	Mean Weighted with Max Power Dist.
Energy [kJ]	499	32	120	175
Maximum Power [kW]	81	11	28	28
Maximum Velocity [mph]	73	21	32	25

Weighted mean is the value obtained by weighting the occurrence frequency of the statistics. This shifts the mean value towards the most frequently appeared value, which is effectively to reflect the central tendency in the distribution profile. The information about energy and maximum power would be the basis for the preliminary design procedure to size the components of the mechanical ESS.

Besides the statistical analysis of actual driving data, a modeling and simulation study is conducted to characterize the dynamic behavior and the energy conversion efficiency of alternative energy storage system (AESS) technologies for parallel hybrid configuration shown in the Figure 13 below.

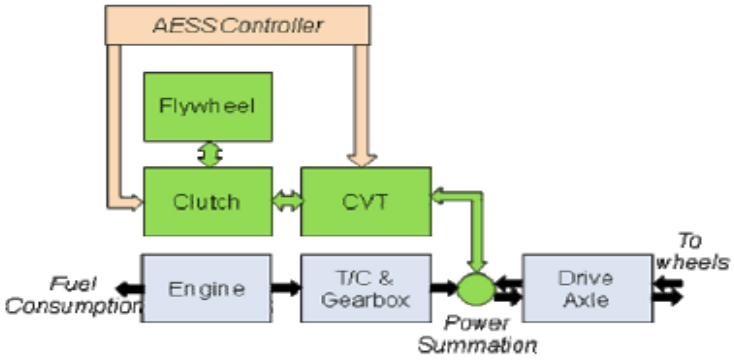

Figure 13: Mechanical Hybrid Powertrain Configuration [11]

Simulation of the mechanical AESS is conducted on the FTP cycle. Figure 14 show the torque commands at the driveshaft, as well as the flywheel speed during the initial portion of the cycle.

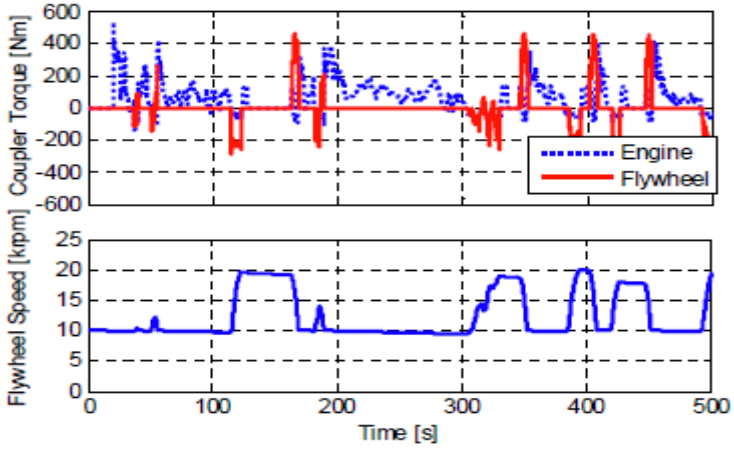

Figure 14: Engine Torque at Driveshaft and Flywheel Speed during the FTP Cycle [11]

An overall energy budget for the mechanical AESS systems is shown in the Figure 15, with a breakdown of the major sources of energy loss. The gear couplings and the clutch-CVT system are sources of energy losses during both the storage and the recovery phase. The friction loss of the flywheel is only marginally relevant [11].

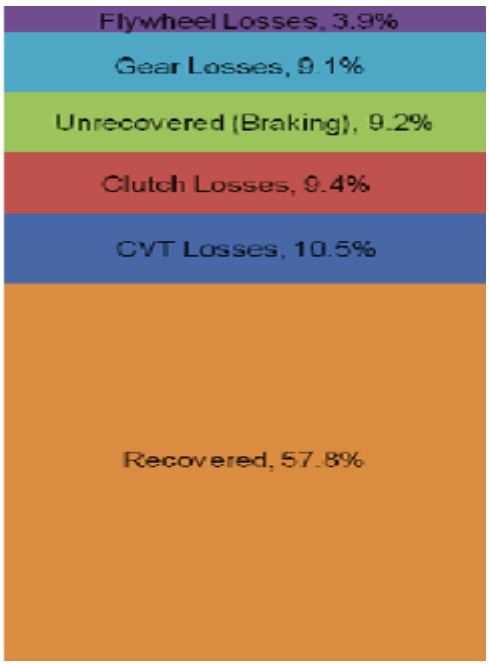

Figure 15: Energy Budget for the Mechanical AESS System [11]

Chapter 3: Design of Scaled Flywheel Prototype

In this chapter, the specifications for the scaled-down prototype in Chapter 2 are revised. The details about the constraints and design procedures of the main components are explained. Then preliminary mechanical and control systems integrations are introduced to show how the flywheel system is assembled and how the system is operated through controlling strategies. Finally, a budget is analyzed in this project.

3.1 Review Specifications for Scaled-down Prototype

The complete flywheel hybrid vehicle can be schematically represented as shown in Figure 16 below. The AESS part of the vehicle architecture includes the flywheel, clutch and CVT. The AESS portion is physically connected to the drivetrain after the transmission. To the AESS part, the vehicle drivetrain is a load that can deliver or accept torque. In the scaled-down prototype, the vehicle part can be assumed as a load represented by a rotational inertia. Hence, the simplified system consists of an inertia representing the vehicle connected in series with CVT, clutch, and flywheel, as shown in Figure 16. The vehicle inertia can transfer energy to the flywheel or receive energy from the flywheel. An electric motor is used to drive the vehicle inertia to simulate the torque initially available at the vehicle driveline.

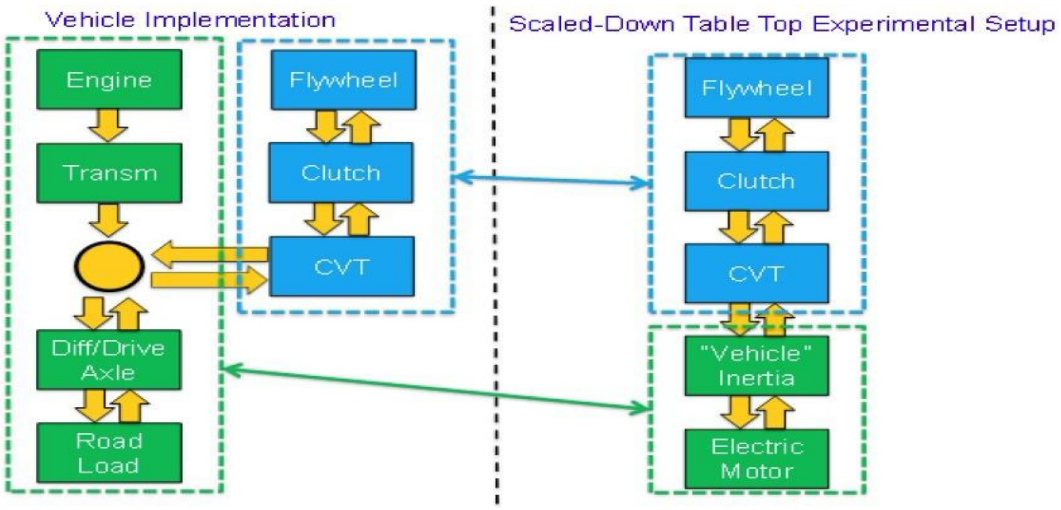

Figure 16: Flywheel Hybrid Prototype Representation

Based on the statistics obtained in Chapter 2, a flywheel system has been designed with power capacity of 28kW and energy rating of 120kJ. For the objective of understanding the system losses and implementing controls, a scaled-down prototype will serve the purpose. A scaling factor of 10 was decided and the scale-down prototype was designed with power capacity of 2.8kW and energy rating of 12kJ.

In the design, the flywheel speed is set to 1000~5000rpm within the range of a typical low-speed flywheel system in the real mechanical hybrid vehicles. The CVT ratio range is 0.333~3 for the speed variator (size 4K) from Cleveland Gear Company. Hence, the vehicle inertia speed is set to 1667~3000rpm. Then the preliminary values of the flywheel and vehicle inertia can be calculated using the equation:

$$I_{fly} = \frac{2*E}{\omega_{fly,max}{}^2 - \omega_{fly,min}{}^2} \quad (3.1)$$

$$I_{veh} = \frac{2*E}{\omega_{veh,max}{}^2 - \omega_{veh,min}{}^2} \quad (3.2)$$

where I is the mass moment of inertia, E is the energy transferred between flywheel and vehicle inertias and ω is the angular speed respectively. The mass moment of inertia of the flywheel is calculated as 0.0912kg·m^2, while that of the vehicle inertia is 0.352kg·m^2. Besides the inertias, the maximum torque that is applied to the flywheel should be considered. In the steady state conditions, the maximum torque transmitted to the flywheel can be obtained based on the power it transmitted and its speed.

$$T_{max} = \frac{P_{max} * 9549}{\omega_{fly,min} * 1000} \quad (3.3)$$

where T is the torque applied to the flywheel in N.m, P is the power transmitted between flywheel and vehicle inertias in kW and ω is the angular speed in rpm. The maximum torque is calculated as 26.74N·m. The design constraints and parameters are tabulated in the Table 3 below.

Table 3: Summary of Design Constraints and Design Parameters

Design Constraints		Design Parameters	
Maximum Flywheel Speed	5000rpm	Flywheel Inertia	0.0912kg·m^2
Minimum Flywheel Speed	1000rpm	Vehicle Inertia	0.352kg·m^2
Maximum Vehicle Inertia Speed	3000rpm	Maximum Torque	26.74N·m
Minimum Vehicle Inertia Speed	1667rpm		

3.2 Main Components

As mentioned in section 3.1, there are four main components in the flywheel based Energy Storage System, which are flywheel inertia, clutch, CVT and vehicle inertia. This section explains the detailed design procedures of these main components.

3.2.1 Flywheel Inertia

Flywheel inertia is the component to store kinetic energy through increasing its rotational speed, and release the energy through deceleration in the mechanical energy storage system. The reverse engineering design process is conducted in the software of Computer Aided Three-dimensional Interactive Application (CATIA).

Flywheel inertia is composed of four parts: main disc, shaft, flange and sensor gear. These parts and the assembled model are shown in the Figure 17 below.

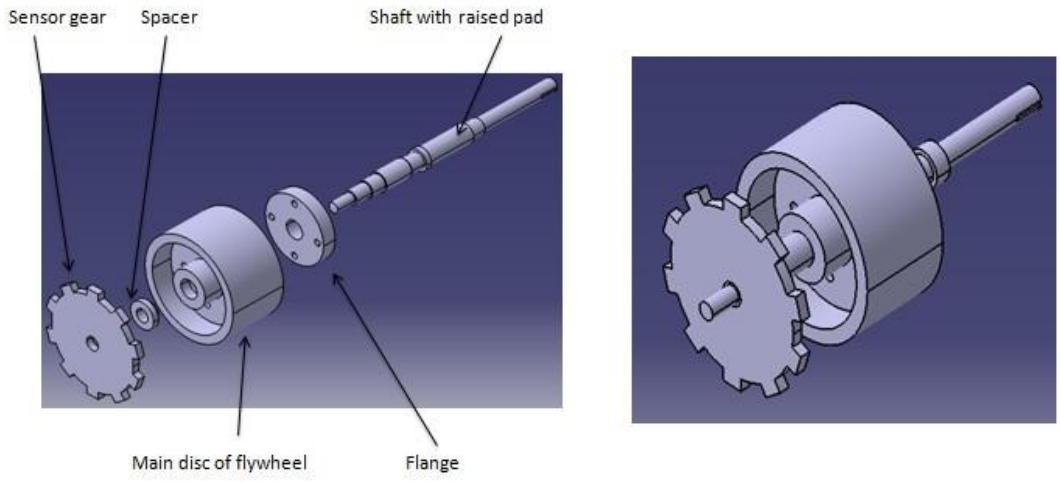

Figure 17: Main Disc, Shaft, Flange and Sensor Gear (Left); Assembled Flywheel Model (Right)

The main disc provides the most of the inertia of the flywheel. The shape of the main disc is a modified cylinder with rim on periphery as shown in the cross-section of the Figure 18 below. This shape is to reduce unnecessary mass around the center axis, therefore diminishing the stress on the bearing supports.

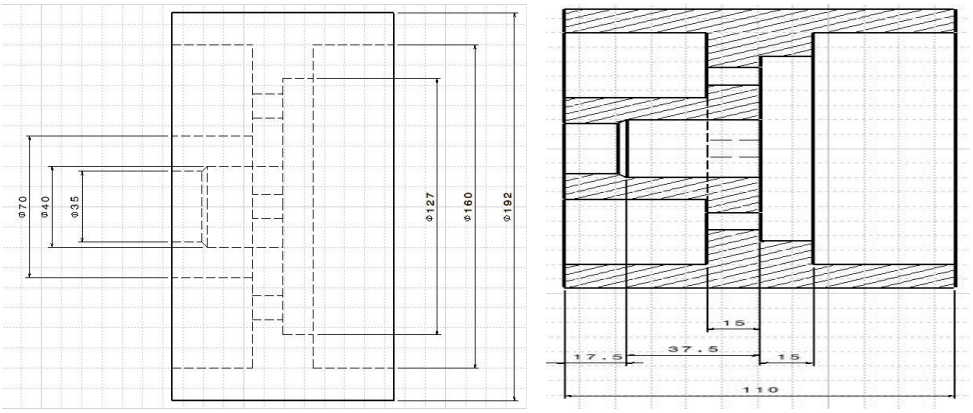

Figure 18: Cross-section of the Main Disc of Flywheel (in mm)

The shaft shown in Figure 19 is designed with the feature of raised pads, which match the inner structures of the main disc to mount it easily.

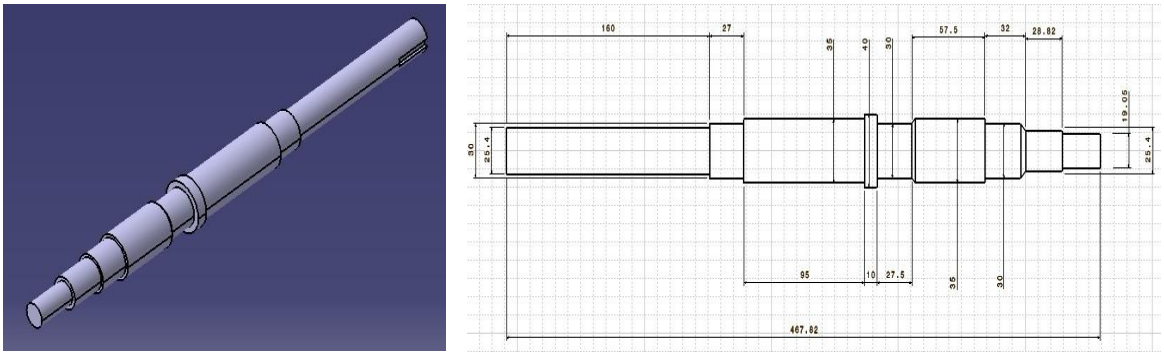

Figure 19: Shaft with Raised Pads (Left); Cross-section of the Shaft (in mm, Right)

The flange (Figure 20) is used to bolt the main disc to hold the disc at a fixed position relative to the shaft. Welding is then performed to create a permanent joint between the flange and the shaft.

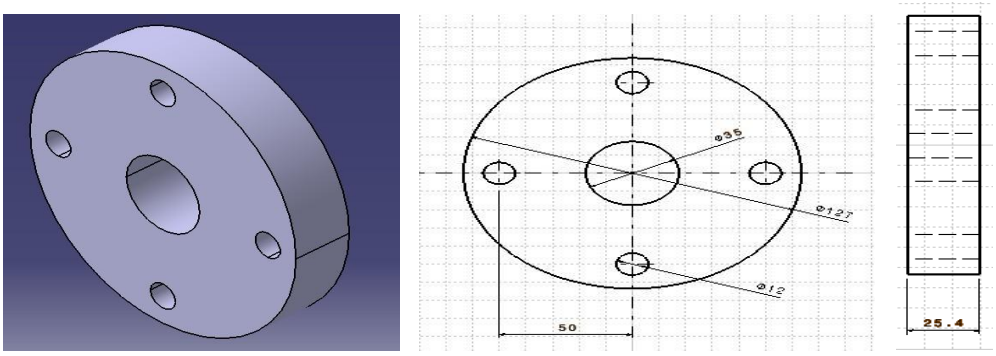

Figure 20: Flywheel Flange (Left); Cross-section of the Flange (in mm, Right)

At one end of the shaft, a sensor gear (Figure 21) is mounted to the shaft. The rotational speed of the sensor gear was measured by a proximity sensor, which was equal to the rotational speed of the flywheel.

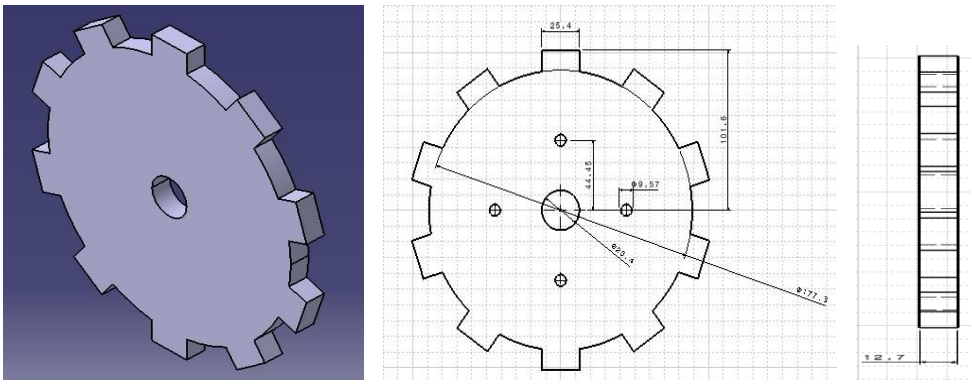

Figure 21: Sensor Gear (Left); Cross-section of the Sensor Gear (in mm, Right)

The Figure 22 below shows the cross-section of the assembled flywheel inertia.

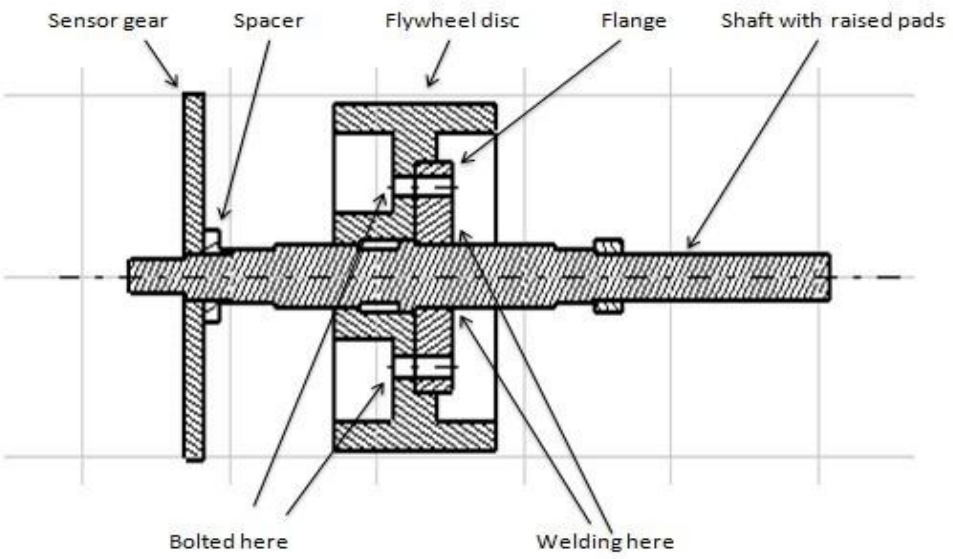

Figure 22: Cross-section of the Assembled Flywheel Inertia

From the viewpoints of cost and machinability, grey cast iron is chosen as the material to fabricate the main inertia. As a ferromagnetic material, cast iron is suitable to fabricate the sensor gear as well. The flange and the shaft are made of steel to ensure that they can tolerate the high stress during rotation. The parameters of the flywheel inertia are shown in the Table 4 below. The total inertia measured through CATIA is 0.0903kg·m^2, which error is 0.97% difference with the desired value.

Table 4: Parameters of the Flywheel Inertia Parts

	Main Inertia	Shaft	Flange	Sensor Gear
Outer Diameter (mm)	192	35	127	205.0
Width (mm)	110	475.9	25.4	12.7
Material	Cast Iron	Steel	Steel	Cast iron
Total Inertia (kg*m^2)	0.0903			

For safety reasons, the maximum stress in the flywheel that exists on the thinnest part of the disc near the rim (Figure 23) should be considered. The maximum stress on the disc can be obtained using the equation 3.4:

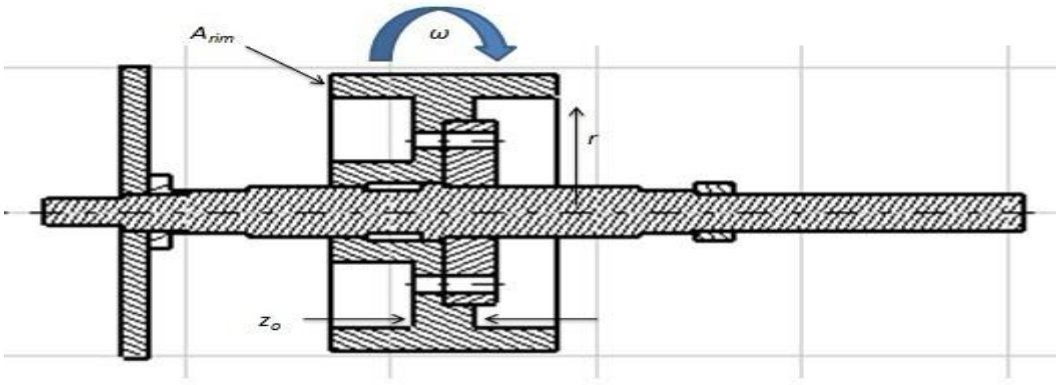

Figure 23: Annotated Cross-section of the Assembled Flywheel Inertia

$$z_o = [\frac{wr^2\omega^2}{g\sigma_o} - (1-v)]\frac{A_{rim}}{r} \quad (3.4)\ [12]$$

where z_o is the thickness of the disc, w is the weight density of the inertia, r is the inner radius of the rim, ω is the angular speed of flywheel, g is the gravity constant, σ_o is the maximum stress that can exist on the disc, v is the Poisson's ratio and A_{rim} is the cross-section area of the rim. The theoretical maximum stress of the disc is calculated as 5.865MPa (850.6psi), while the yielding stress of the cast iron is 111.8MPa (16215psi). Hence, the flywheel inertia design has a factor of safety of 19, which means the design is quite reliable.

3.2.2 Clutch

Clutch is the component to couple the flywheel inertia and the vehicle inertia when the CVT is at certain ratio range, particularly engaging while the flywheel is accelerating from rest and disengaging while the flywheel is rotating and the vehicle is at rest. Torque is transferred through clutch between the flywheel inertia and vehicle inertia. Hence, the power transmitted in the flywheel system can be controlled by a clutch that could continuously manipulate the torque.

The clutch chosen for the flywheel system is L-600 Pilot Mount Clutch from Nexen Group. The maximum torque it transmitted is 41.80N-m, which is greater than the maximum torque required. It can also attain a maximum power of 7.5kW that is greater than our designed value of 2.8kW. The pneumatic clutch is designed for air actuation and spring return with a minimum engage pressure of 5psi and a maximum pressure supply of 80psi. Figure 24

below shows the linear relationship between air pressure and torque supplied. Varying the air supply pressure from 5 to 80psi, the clutch can control torque transmitted from 0 to 370lb-in (41.80N-m). Once the air pressure is quickly released below 5psi, the clutch will disengage the flywheel inertia from the vehicle inertia.

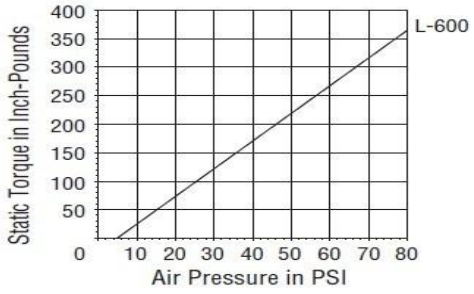

Figure 24: Static Torque vs. Air Pressure [13]

Since the clutch does not have a coupling half, the coupler shown in Figure 25 is designed to connect the clutch and the CVT. A sensor gear, which is identical to that in the flywheel should be installed at the end of the coupler, to measure the rotational speed of the clutch on the side near the CVT. Figure 26 shows the parts of the clutch and the assembled model.

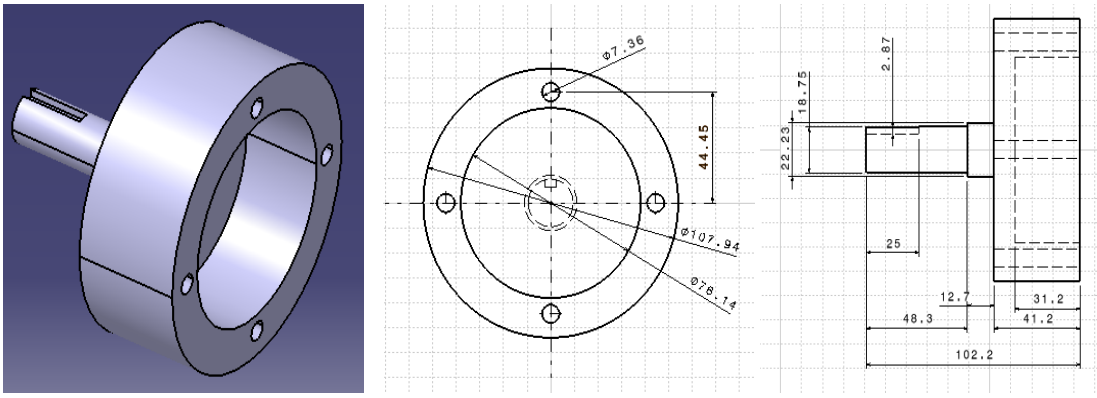

Figure 25: Clutch Coupler (Left); Cross-section of the Coupler (in mm, Right)

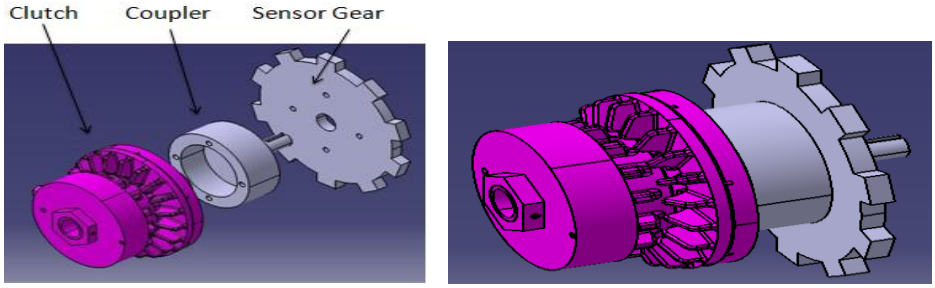

Figure 26: Parts of the Clutch Model (Left); Assembled Model (Right)

A control valve system is designed to control the air supply pressure to the clutch, therefore manipulating the maximum power transmitted in the flywheel system. This will be described in the Chapter 3.4.1, together with the flywheel system control hardware.

3.2.3 Continuously Variable Transmission (CVT)

A continuously variable transmission (CVT) is a transmission component that can change ‘steplessly’ through an infinite number of effective gear ratios between maximum and minimum values. CVT ratio is defined as the ratio of rotational speed of the flywheel inertia to the rotational speed of the vehicle inertia. Any change in the CVT ratio can be viewed as the transfer of kinetic energy between the flywheel inertia and vehicle inertia.

To satisfy our design parameters and budget, we choose the speed variator (size 4K) from Cleveland Gear Company. It is a dependable, compact, mechanical drive that provided infinitely variable output speeds over a range from 0.333 to 3. Figure 27 below shows the pictures of the frame and inner structure of the speed variator.

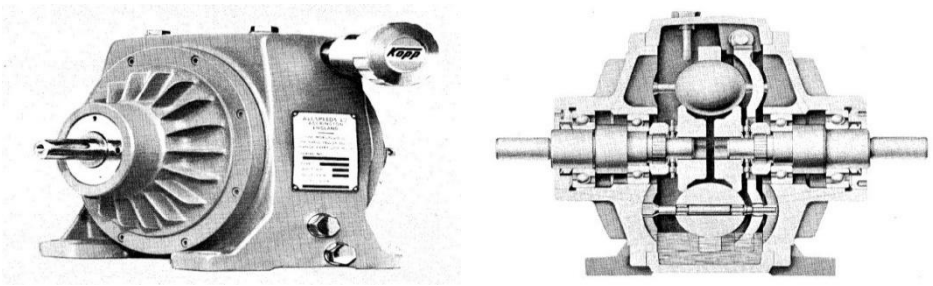

Figure 27: Variator Frame (Left) & Inner Structure (Right) [14]

In the variator, the CVT ratio can be changed by tilting the ball axis by a handwheel, which varied the ratio of the relative lengths of the contact paths on the input and output sides of the balls [14]. This process to change the CVT ratio is illustrated in the Figure 28 below.

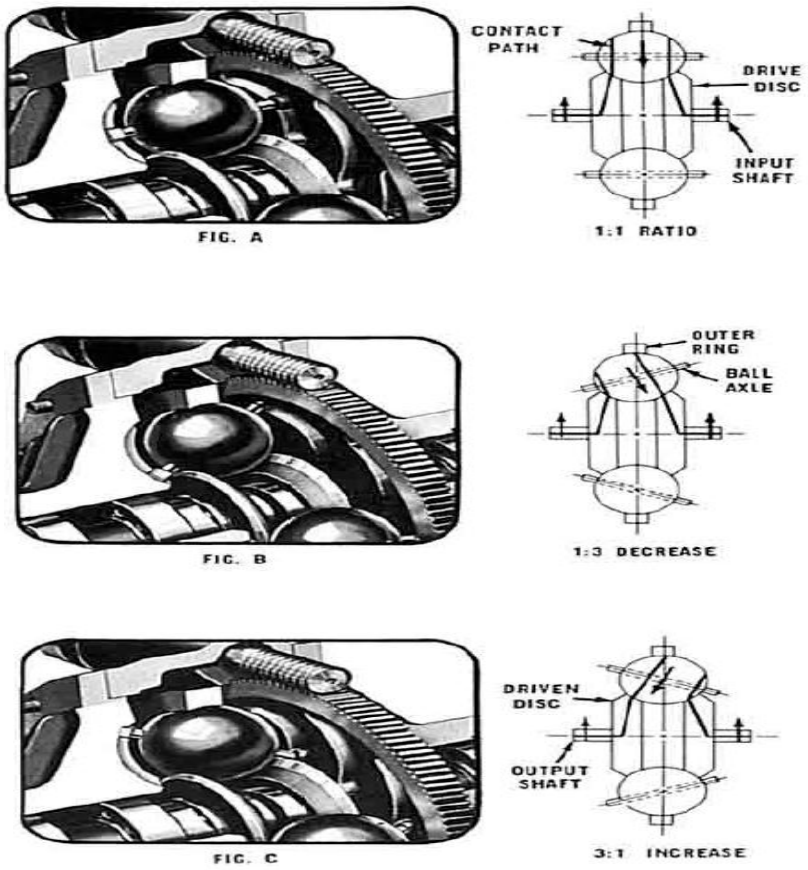

Figure 28: Process of the Change of the CVT Ratio [14]

There is a nearly linear relationship between handwheel turns and the CVT ratio. From the Figure 29 below, the CVT ratio is 1/3 at the initial handwheel position; while it increases linearly to 3 after 20 turns of the handwheel. A step motor will be needed to control the CVT speed ratio through turning the handwheel. It will be discussed in the Chapter 3.4.2 later.

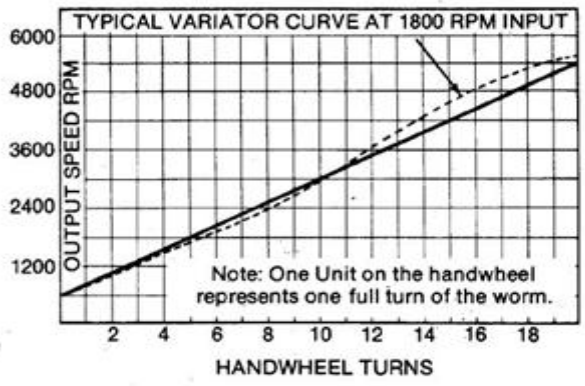

Figure 29: Output Speed at 1800 rpm Input vs. Handwheel Turns [14]

3.2.4 Vehicle Inertia

The vehicle inertia is the component representing the tendency of the vehicle to resist any change in its motion. The reverse engineering design process which is the same used for the flywheel system, will be used to design the vehicle inertia, using the CATIA.

There were also four parts of the vehicle inertia model, which are the main disc, the shaft with raised pads, the flange and the sensor gear. These parts and the assembled model are shown in the Figure 30 below.

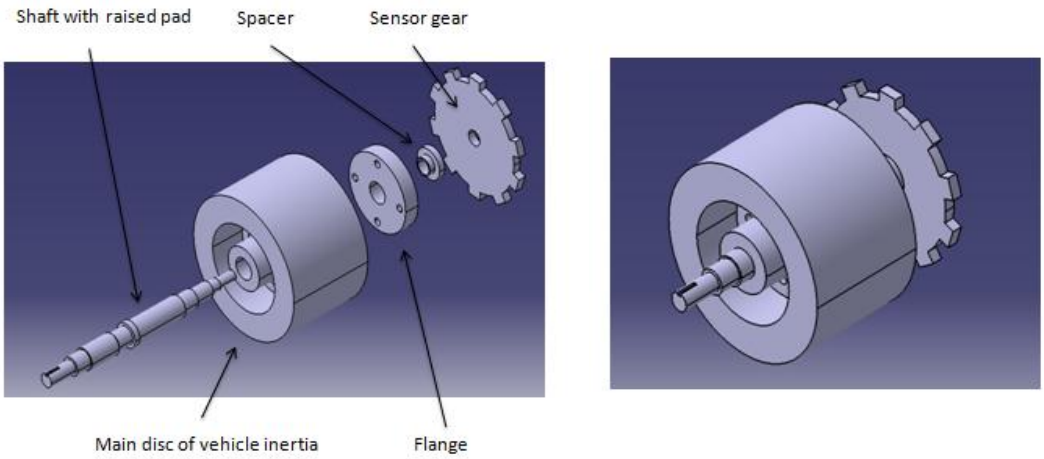

Figure 30: Main Disc, Shaft, Flange and Sensor Gear (Left); Assembled Vehicle Inertia Model (Right)

The main disc of vehicle inertia has the similar shape but different dimensions to provide a larger inertia than the flywheel (Figure 31). The shaft is also designed with raised pads to fit the inner structure of the main disc (Figure 32).

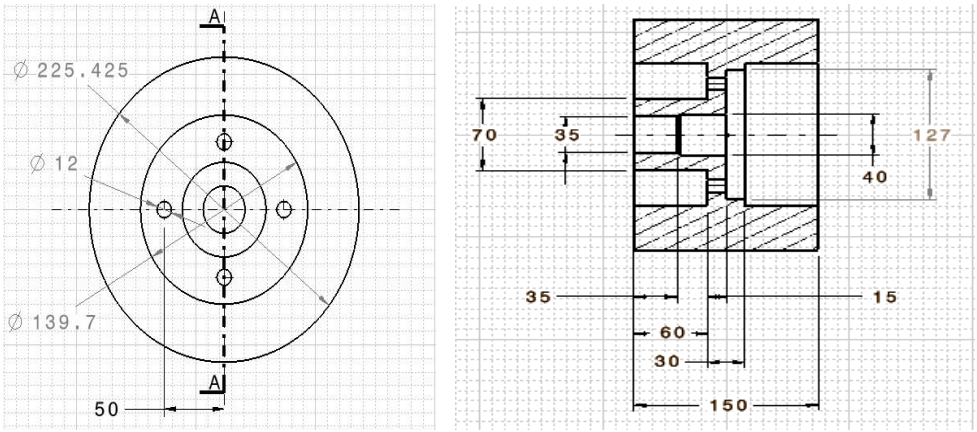

Figure 31: Cross-section of the Main Disc of Vehicle Inertia (in mm)

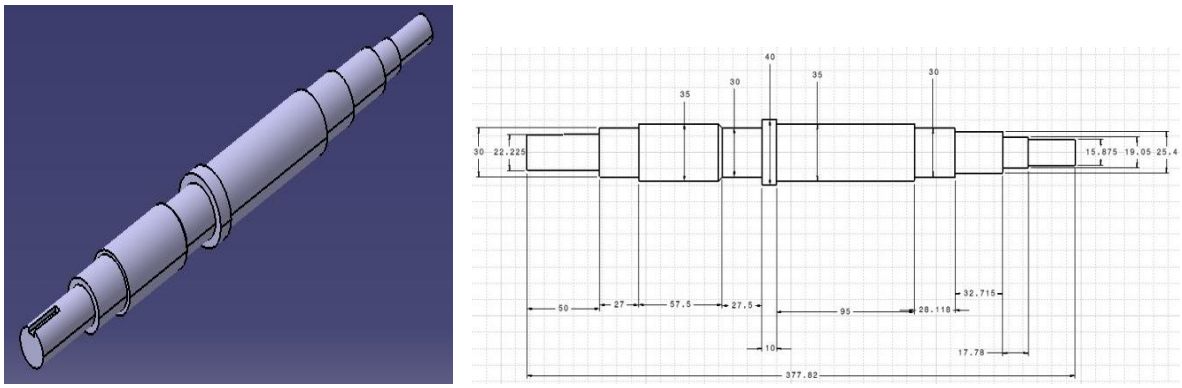

Figure 32: Shaft with Raised Pads for Vehicle Inertia (Left); Cross-section of the Shaft (in mm, Right)

The flange and the sensor gear in the vehicle inertia are identical to those in the flywheel inertia. The Figure 33 below shows the cross-section of the assembled vehicle inertia.

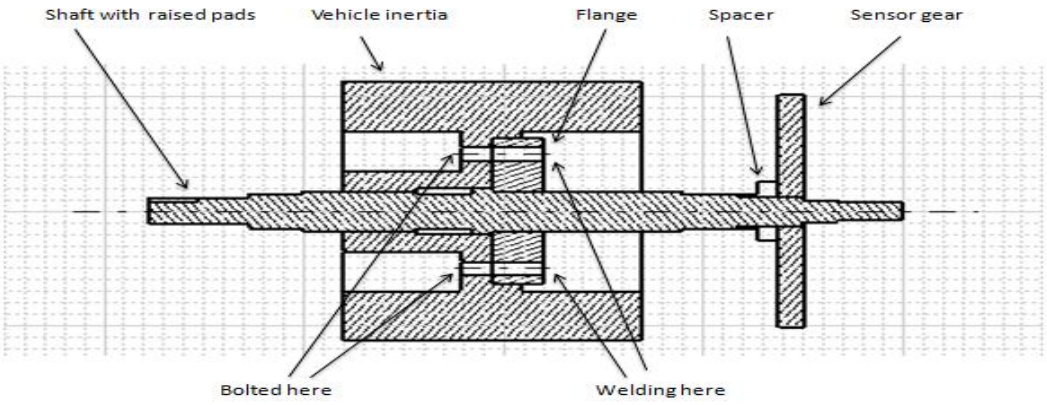

Figure 33: Cross-section of the Assembled Flywheel Inertia

As for the flywheel inertia, grey cast iron is chosen as the material to fabricate the main inertia and the sensor gear. The flange and the shaft are made of steel to ensure they can tolerate the high stress during rotation. The parameters of the vehicle inertia are shown in the Table 5 below. The total inertia measured through CATIA is 0.358kg·m^2, which error is 1.79% difference with the desired value.

Table 5: Parameters of the Vehicle Inertia Parts

	Main Inertia	Shaft	Flange	Sensor Gear
Outer Diameter (mm)	225.4	35	127	205.0
Width (mm)	150	377.8	25.4	12.7
Material	Cast Iron	Steel	Steel	Cast iron
Total Inertia (kg*m^2)	0.358			

The maximum stress on the thinnest part of the disc near the rim can be obtained using the previous equation 3.3. The theoretical maximum stress of the disc is calculated as 3.106MPa (450.5psi), while the yielding stress of the cast iron is 111.8MPa (16215psi). Hence, the flywheel inertia design has a factor of safety of 36, which means the design is quite reliable.

3.3 Mechanical System Integration

After the individual component is procured, they should be connected together to form a whole system. This section of mechanical system integration explains the design of the shaft couplings, the bearing boxes and the frame.

3.3.1 Shaft Couplings

To connect the shafts that connected to each component, shaft couplings are used to join them together. Multi-flex shaft couplings are ordered from McMaster-CARR Company. The coupling shown in Figure 34 below is consisted of two parts: the steel hubs with standard bore sizes and the rubber element "sandwiched" between two hubs.

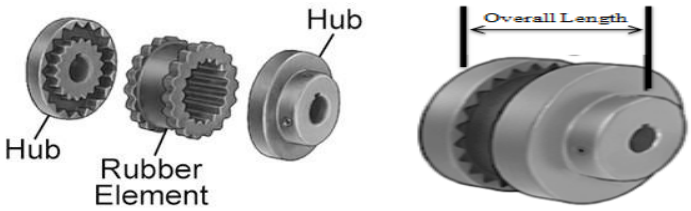

Figure 34: Multi-flex Shaft Coupling Parts (Left); Assembled Model (Right)

Unlike normal couplings that rigidly connect the shafts, the Multi-flex shaft couplings have rubber elements inside to connect the metal hubs. The rubber feature makes the couplings to take on parallel, angular, and axial misalignment plus dampen vibration and shock. The torque limit it can transfer is 50.8N·m (450lb-in), which is larger than the previously calculated maximum static torque (26.74N·m). The parameters of the couplings are shown in the Table 6 below.

Table 6: Parameters of the Multi-flex Shaft Coupling

Bore Size:	5/8 to 1 in		
Bore Depth:	17/32 in		
Overall Length:	35/16 in		
Hub Outer Diameter:	4 in		
Torque Limit:	50.8 N·m		
Maximum Speed:	6000 rpm		
Maximum Misalignment:	0.015 in (Parallel)	1° (Angular)	0.125 in (Axial)

3.3.2 Bearing Boxes

Bearings are used to support the shafts, while allowing free rotation of these shafts. The bearings chosen are self-aligning ball bearings of the model 2206E-2RS1TN9 from Svenska Kullagerfabriken (SKF) Company. The bearings have two rows of balls and a common concave sphere raceway in the outer ring. Since the bearings are consequently self-aligning and insensitive to angular misalignments, they are particularly suitable for the assembly of the flywheel system where considerable shaft deflections or misalignment are expected. In addition, the bearings have the lowest friction of all rolling bearings, which enables it to generate less heat at high speed operation. Figure 35 below the bearing and its drawing.

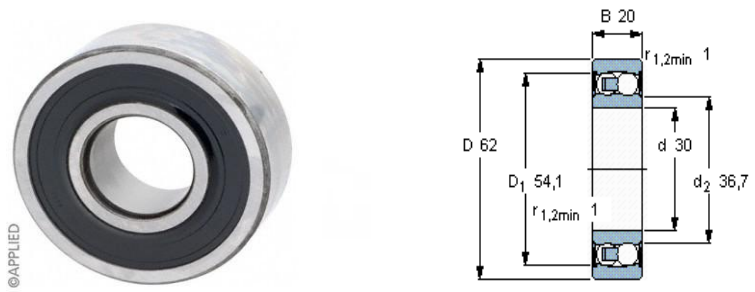

Figure 35: SKF Bearing (Left) and Drawing (in mm, Right)

To appropriately contain the bearings, bearing boxes are designed in order to support the flywheel system in a frame. The parts of the bearing box and the assembled model are presented in the Figure 36 below. The feature of tab is adopted in the box plates to allow easy assembly. The holder and spacer are bolted by screws to keep the bearing at the fixed position. Shoulder screws are used to hold the bearing box in the frame.

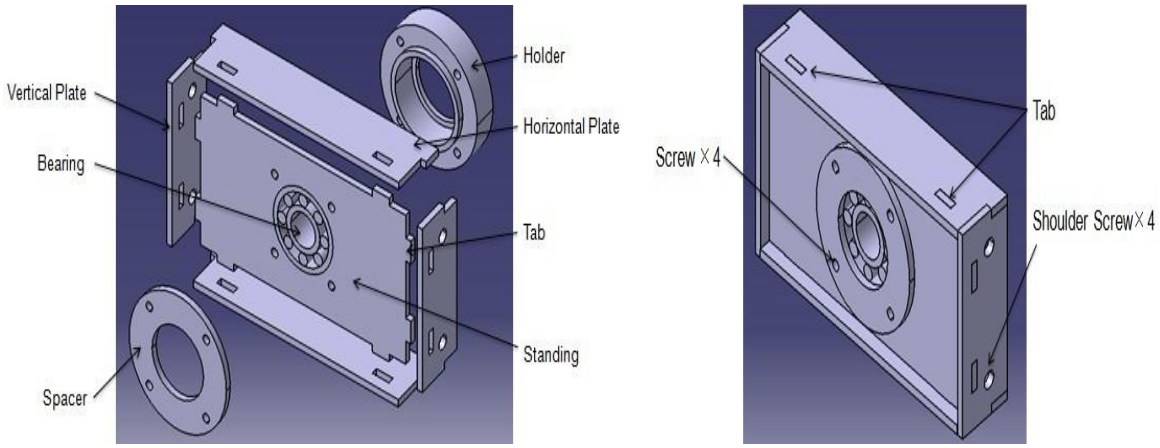

Figure 36: Parts of the Bearing Box (Left); Assembled Model (Right)

3.3.3 Frame

For safety reasons, a metallic frame should be designed to secure each component in appropriate places. The frame is mainly consisted of three parts: top plate, side plates, bottom plate. The plates are hollowed out to reduce the weight. Gussets are adopted to strengthen the stability of the frame. The Figure 37 below shows the frame model and detailed drawings.

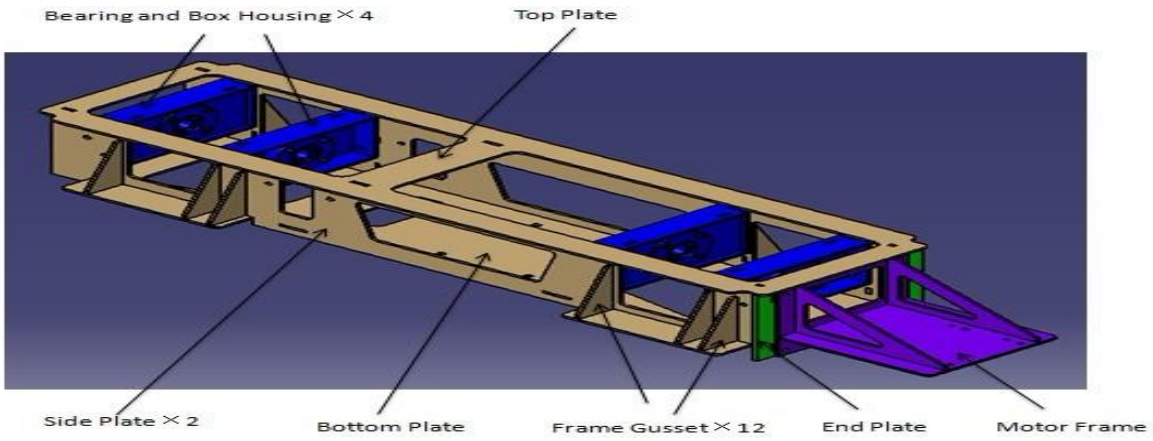

Figure 37: Frame Model

The detailed drawings of the plates are presented in the Figure 38-40 below.

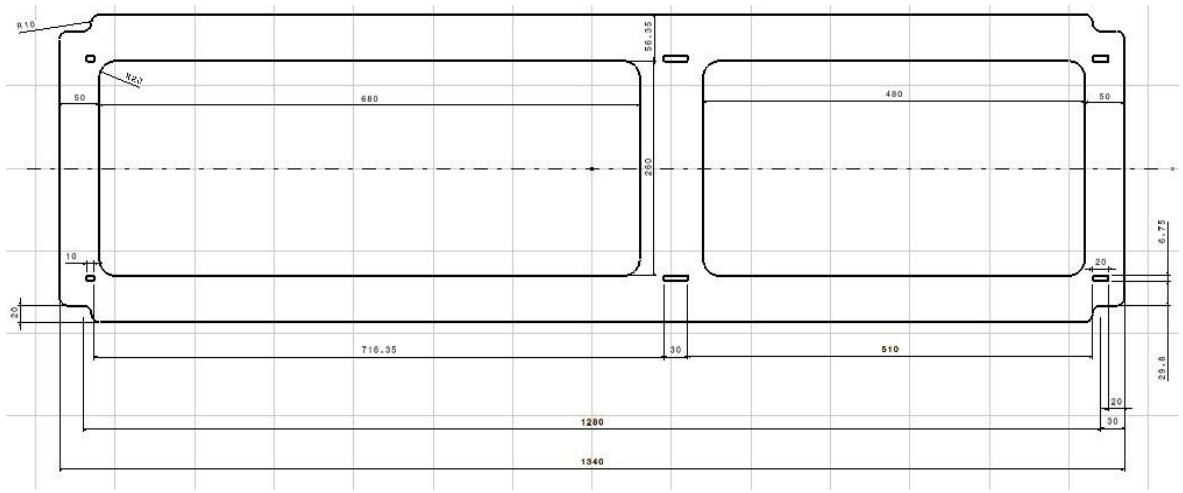

Figure 38: Top Plate Drawing (in mm)

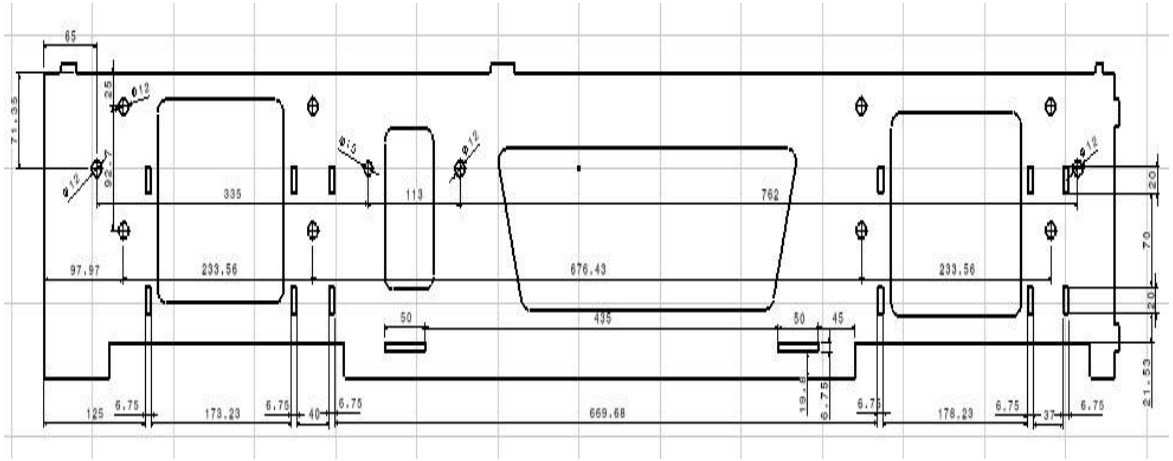

Figure 39: Side Plate Drawing (in mm)

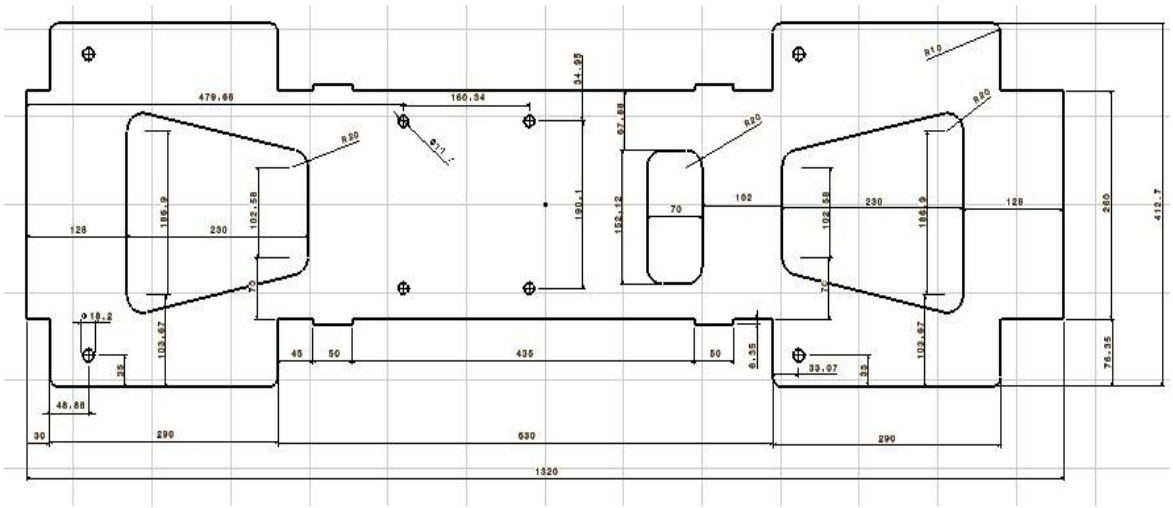

Figure 40: Bottom Plate Drawing (in mm)

Finally, the flywheel system is assembled after procuring each component. The Figure 41 below shows the overview of the mechanical parts of the flywheel system.

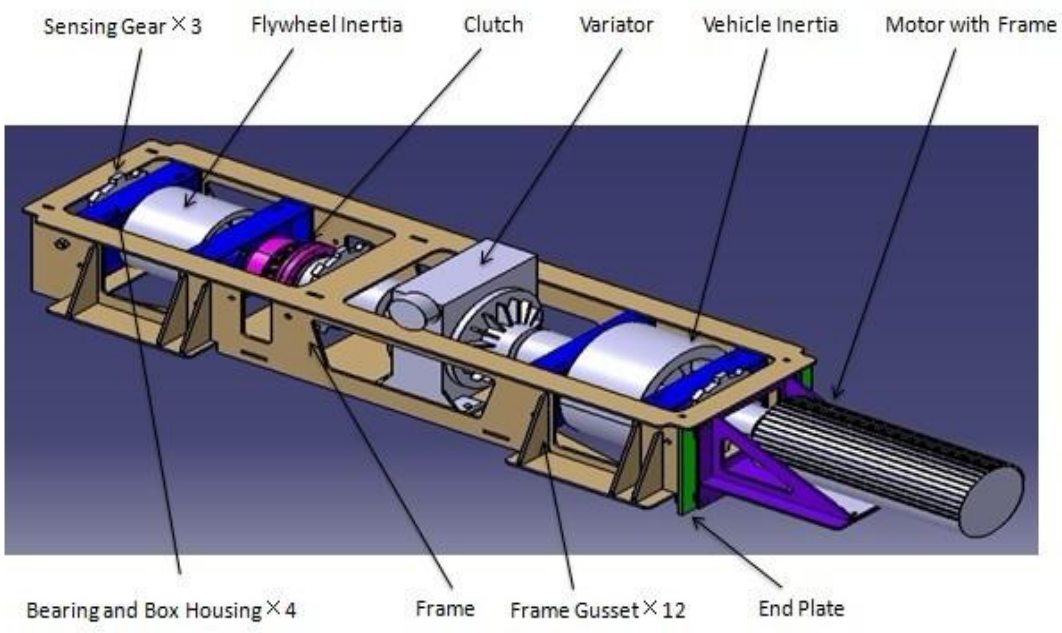

Figure 41: Assembled Flywheel System

3.4 Control System Integration

The control system includes three parts: the actuation for the clutch engagement, the actuation for the change of the CVT ratio and the speed sensing system. The clutch engagement is controlled by operating a proportional valve that pressurizes the clutch pneumatically. The CVT ratio is controlled by a stepper motor, through turning its hand wheel. The Figure 42 below shows the schematic of the actuation system adopted for the flywheel prototype.

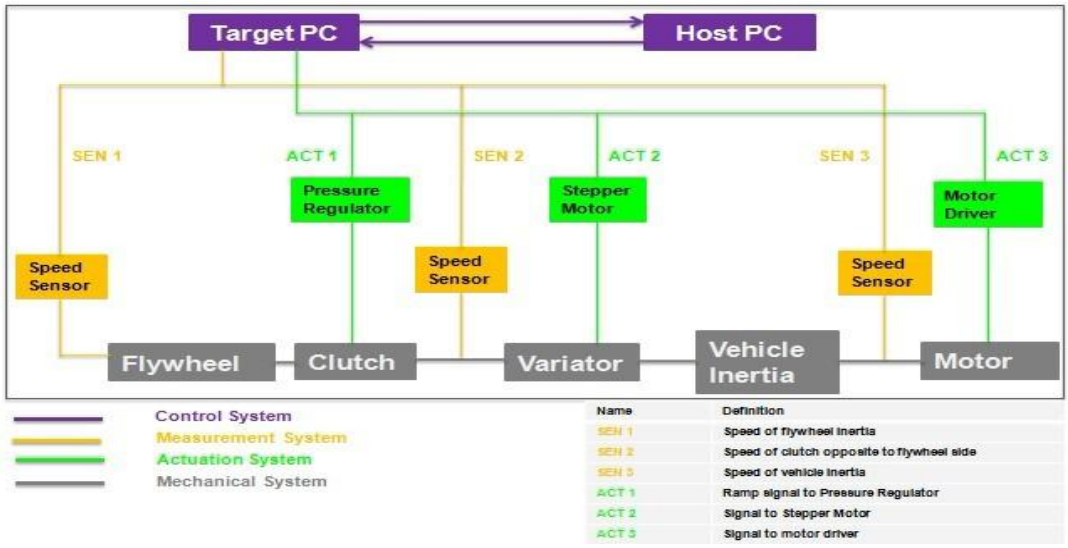

Figure 42: Overview of the Control Systems

3.4.1 Actuation for Clutch System

As mentioned previously in Chapter 3.2.2, the flywheel system is equipped with a pneumatic clutch. The schematic of the clutch actuation system is shown in Figure 43. By means of varying the clutch chamber control pressure, different levels of torque transmitted, from the CVT to the flywheel and vice versa, can be achieved.

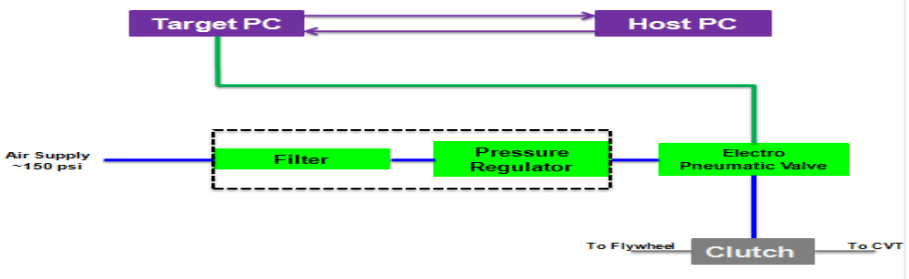

Figure 43: Schematic of the Clutch Actuation System

In order to accurately drive the clutch, a proportional electronically controlled flow valve was used. This valve should finely regulate the output pressure by means of a proportional analogical control signal. The clutch pressure is varied to transfer desired torque through the clutch. The control valve chosen is Type 500X Electro-Pneumatic Transducer with the model number 4993K4 from McMaster-CARR Company. The characteristic linear actuation curve is presented in the Figure 44 below.

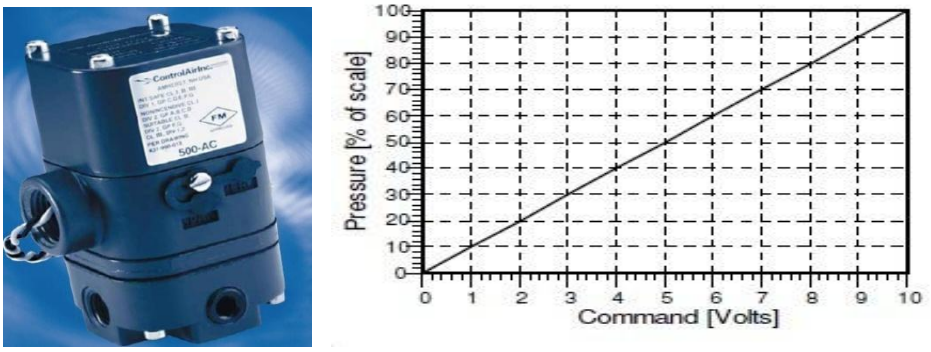

Figure 44: Type 500X Electro-Pneumatic Valve (Left); Characteristic Linear Actuation Curve (Right) [15]

3.4.2 Actuation for CVT System

The CVT actuation system primarily includes the actuation of a stepper motor to obtain desired CVT ratio. The stepper motor turns the hand wheel to apply automatic control. Figure 45 below shows the overall layout of the CVT system.

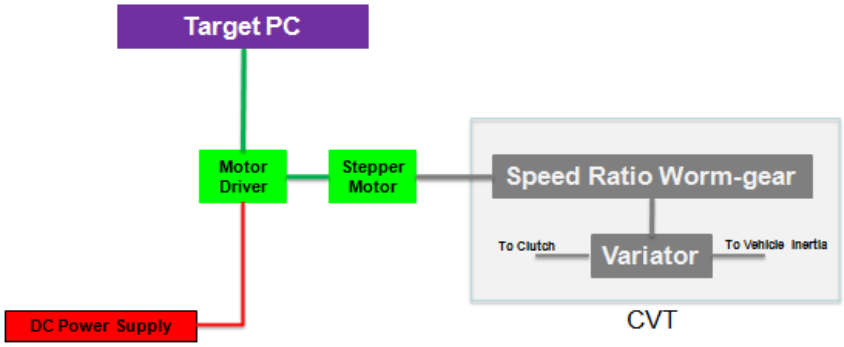

Figure 45: Schematic of the CVT Actuation System

The stepper motor is used to operate the hand wheel in the CVT variator. The motor is connected to the hand wheel using a mechanical joint. The motor requires the clock pulse input that indicates the frequency of rotation. The motor torque-speed characteristics are given in Figure 46 below.

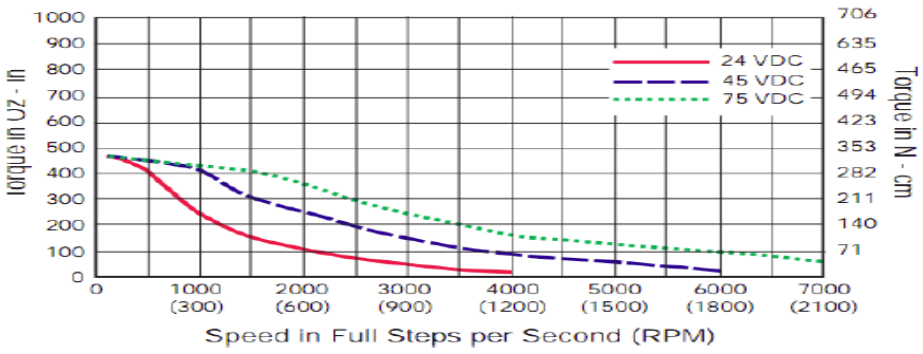

Figure 46: Stepper Motor Characteristic Curve

3.4.3 Speed Sensing System

The speed sensing system mainly incorporates three non-contact inductive speed sensors from Omega Engineering Incorporation and designed tooth gears fixed at three locations of the assembly. The sensors are fixed at a distance of 2mm from the toothed gears. The sensors generate a high voltage when they reach the addendum of the gears and a low voltage when they reach the dedendum of the gears. Hence, the sensors generate a square wave pulse signal that can be processed to measure rotational speeds. Figure 47 below shows the speed sensing system.

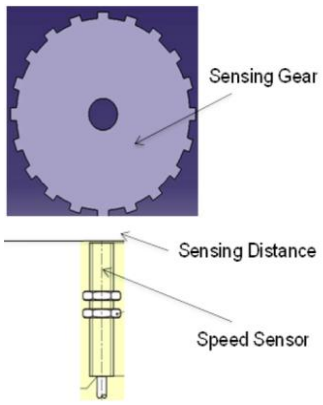

Figure 47: Speed Sensing System [16]

In the prototype, the speed sensors are installed in three locations where the sensing gears are present. This has been shown in the previous Figure 41. Post-processing of sensor output is required to compute the rotational speed. This involves counting the number of rising edges of the sensor pulses using a Simulink Counter Block and finding the speed based on the counts.

3.5 Budget

The design of a scaled down flywheel prototype is a part of the project "Alternative Energy Storage System", which is sponsored by General Motor Corporation. A budget should be analyzed during the design process. The Table 7 below presents the budget spent in the design of the flywheel system. Overall, the budget of the project is around $10942.8.

Table 7: Budget of Prototyping a Low Speed Flywheel System

Ordered Parts	Description	Unit Price/ $	Quantity	Price/ $
Bearing	Self-aligning Ball Bearing from SKF	133.53	4	534.12
Shaft Couplings	Multi-flex shaft coupling	56.63	3	169.89
Materials	Materials to fabricate Shaft and Inertia			882.12
Control Valve	4993K4 Low Flow Electronic Air Regulator	309.41	1	309.41
Air Filter	4910K22 Space-Saver Stacked Filter/Regulator	43.81	1	43.81
Speed Sensor	PROXIMITY SENSORS PRX102-12N	95.00	3	285.00
Air Dryer	Desiccant Air Dryer 5163K22	180.48	1	180.48
Oil Remover	Filter, Oil Removal 4ZL24	118.17	1	118.17
Tubing	Tubing to connect Clutch Actuation System			97.01

Clutch	L-600 805283 Pilot Mount Nexen Clutch	404.85	1	404.85
CVT	4K Speed Variator from Cleveland Gear Company	5,100	1	5,100
Laser Flex	Fabricate components from Laser Flex Corporation			1,317.94
MATHWORKS	Computer Softwares			1,500
			Total	10,942.8

Chapter 4: Tests and Results

As a part of a large project conducted at the Ohio State University, the low-speed flywheel prototype is used to demonstrate a typical energy recovery process in hybrid flywheel vehicles. This experimental work is done by Kingsly Jebakumar. I mention it in this chapter to explain the performance of the designed flywheel systems.

4.1 Tests

In the tests, the vehicle inertia is charged to 2500rpm initially. Then signal commands are given to actuate clutch and CVT to demonstrate the energy recovery process. The Figure 48 shows the desired CVT ratio and the desired clutch pressure which are the actuation command computed by the model.

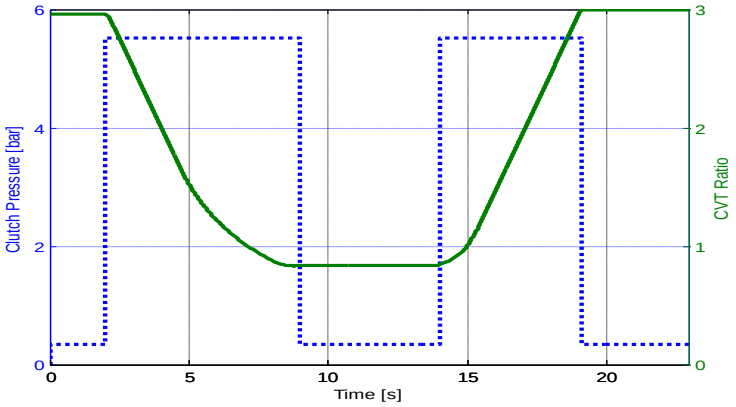

Figure 48: Actuation Commands for the Clutch and CVT [17]

This clearly indicates the pressure rise during the clutch engagement events and the pressure drop during the clutch disengagement events. The desired change in the CVT ratio is shown, which increases during the regeneration phase and decreases during the drive phase, to maximize the energy transfer [17].

4.2 Results

The speed profiles are recorded for the flywheel and vehicle inertias. They are compared with a simulation model. The Figure 49 and 50 below shows the speed profiles of the flywheel and vehicle inertias in both simulation and experiment.

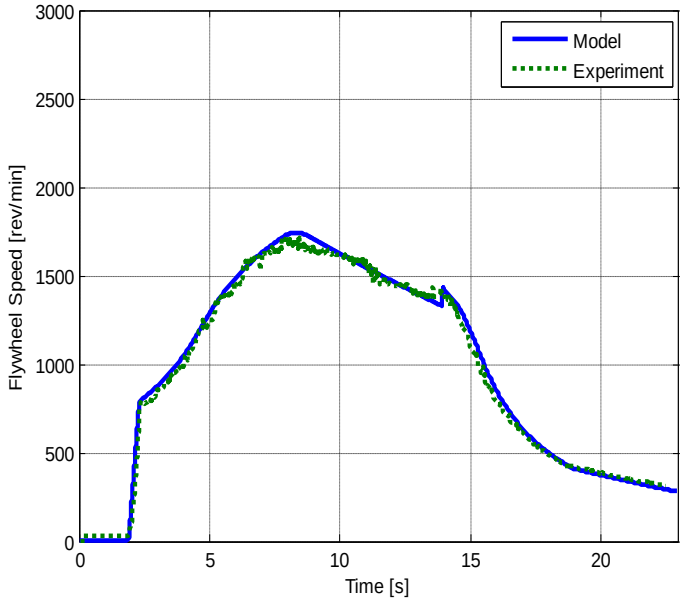

Figure 49: Speed Profile of Flywheel Inertia in Simulation and Experiment [17]

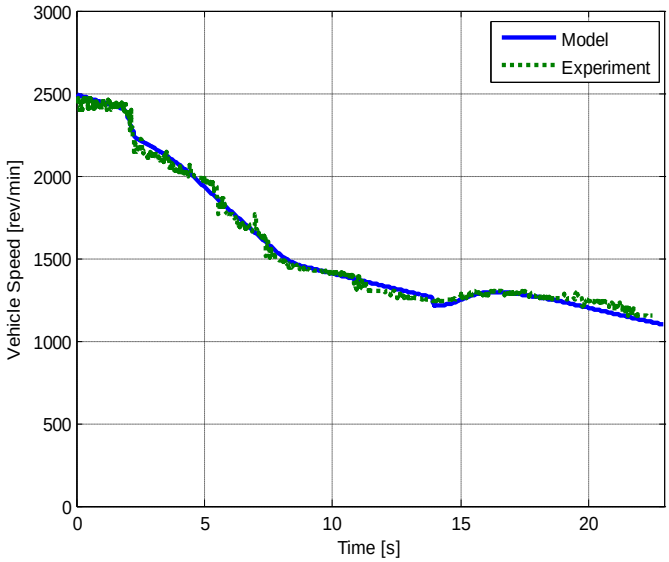

Figure 50: Speed Profile of Vehicle Inertia in Simulation and Experiment [17]

The speed profiles clearly show that the flywheel speed increases and the vehicle inertia speed rapidly decreases during the 2-8s. It indicates that the flywheel can act as a brake to absorb the kinetic energy of the vehicle inertia. During the 8-14.5s, the clutch is disengaged and both the flywheel and the vehicle inertia speeds decrease. It shows that friction and aerodynamic drag force exist in the designed prototype. The flywheel speed decreases and the vehicle inertia speed increases slightly during the 14.5-19s. It demonstrates the process of the energy recovery to the vehicle inertia during acceleration. Though the simulation model does not exactly match the speed profiles of the flywheel and vehicle inertias, it can reflect the essential trends of the flywheel and vehicle inertia speeds during various phases.

To further analysis the energy transfer between the flywheel and vehicle inertias, the kinetic energy profiles of both flywheel and vehicle inertias are shown in the Figure 51 and 52 below.

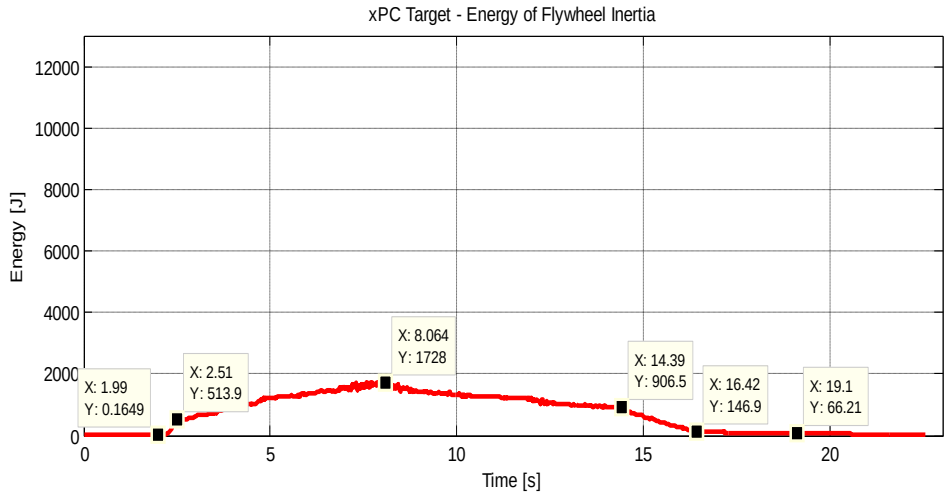

Figure 51: Kinetic Energy Profile of Flywheel Inertia in the Experiment

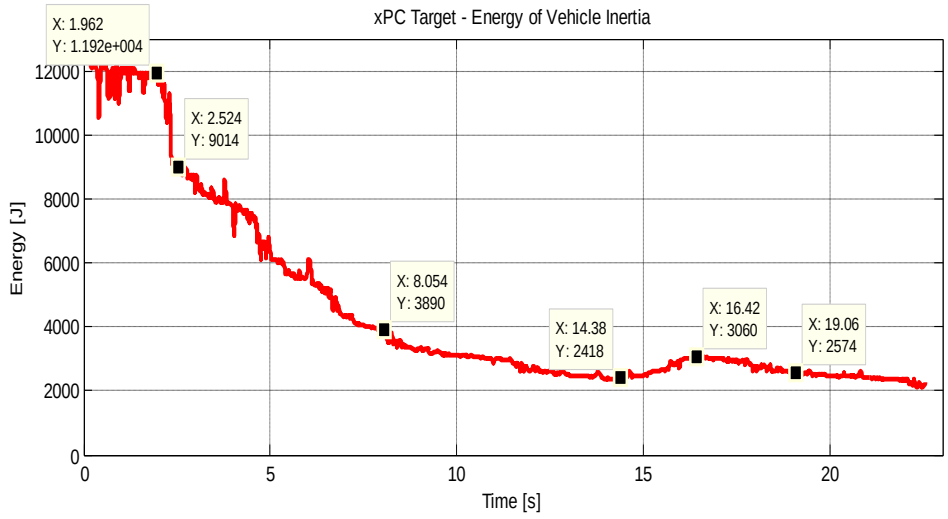

Figure 52: Kinetic Energy Profile of Vehicle Inertia in the Experiment

During 8-14.5s, the power losses of both flywheel and vehicle inertias due to friction can be obtained through the equations below.

$$P_{loss,fly} = \frac{\Delta KE_{fly}}{\Delta T} \quad (4.1)$$

$$P_{loss,veh} = \frac{\Delta KE_{veh}}{\Delta T} \quad (4.2)$$

$$P_{loss,fric+aero} = P_{loss,fly} + P_{loss,veh} \quad (4.3)$$

where P_{loss} is the power loss in W, ΔKE is the change in kinetic energy in J during the time interval and ΔT is the time in s. The power loss of the flywheel due to friction and aerodynamic drag force is calculated as 130W; and the power loss of the vehicle inertia is calculated as 233W. These values reflect how much energy is dissipated per unit time due to friction and aerodynamic drag force in flywheel and vehicle inertias. The total power loss at this stage is estimated as 363W.

During the clutch engagement process from 2-2.5s, the energy loss due to clutch slipping can be obtained from the equation below.

$$\Delta KE_{veh} = \Delta KE_{fly} + E_{loss,clutch\ slipping} \quad (4.4)$$

where E_{loss} is the energy loss in J. The energy loss due to clutch slipping in the clutch engagement process is obtained as 2392J.

During 2.5-8s, the energy loss due to friction and aerodynamic drag can be obtained through the energy balance equation below.

$$\Delta KE_{veh} = \Delta KE_{fly} + E_{loss,fric+aero} \quad (4.5)$$

The total energy loss at this stage is estimated as 3910J. The total power loss is estimated as 707W, which is much higher than the value obtained at the stage of the disengagement during 8-14.5s. The reason may be that the vehicle inertia is charged to a maximum rotational speed initially, which friction and aerodynamic drag are also at the maximum. The efficiency of the energy transfer process to charge the flywheel at this stage is about 23.7%.

Similarly, an energy balance analysis can be conducted during 14.5-19s to obtain the energy loss due to friction and aerodynamic drag force.

$$\Delta KE_{veh} = \Delta KE_{fly} - E_{loss,fric+aero} - E_{loss,clutch\ slipping} \quad (4.6)$$

We can assume that $E_{loss,clutch\ slipping}$ is at minimum because the ratio of the flywheel to vehicle inertia speeds is close to the CVT ratio, which little energy is wasted in the slipping. The total energy loss due to friction and aerodynamic drag force at this stage is estimated as 684J. The total power loss is estimated as 146W, which is smaller than the value obtained at the stage of the disengagement during 8-14.5s. The result confirms that the friction and aerodynamic drag are larger when the vehicle inertia is at a higher rotational speed. The efficiency of the energy transfer process from flywheel to vehicle inertia (14.5-16.5s) at this stage is about 84.5%.

Multiplying the two efficiencies for the energy transfer processes, we can obtain the efficiency for two-way energy transfer. The two-way efficiency is about 20.0%, which is reasonable. However, the overall energy recovered to the vehicle inertia at the end is about

156J from a total energy loss of 9502J. The overall efficiency is only about 1.6%, which is significantly low. The energy loss due to the friction and aerodynamic drag is about 6888J (72.5%); the energy loss due to the clutch slipping is about 2392J (25.2%); and the energy of 66J (0.7%) is still remaining as the kinetic energy in the flywheel. The results of the energy analysis are summarized in the Table 8 below.

Table 8: Summary of the Energy Analysis of the Processes at Each Stage

Stage/s	ΔKE_{veh}/J	ΔKE_{fly}/J	$E_{loss,fric+aero}$/J	$E_{loss,clutch\ slipping}$ /J
2-2.5s	2906	514	-	2392
2.5-8s	5124	1214	3910	-
8-14.5	1472	821	2294	-
14.5-19	156	840	684	-
Overall	9346	66	6888	2392

From the result, we can conclude that the friction and aerodynamic drag force are the major factor to lower the efficiency of the designed flywheel prototype. To improve the efficiency, the flywheel can be placed in a vacuum box to reduce aerodynamic drag force to minimum. High-efficient bearings and couplings can also be applied to reduce the friction in the prototype. The clutch can be engaged faster with a higher pressure to reduce the energy wasted in the slipping.

Chapter 5: Conclusion and Future Works

In this project, a prototype of a low-speed flywheel system was designed to demonstrate the automotive brake energy recovery process. Literatures from prior works were reviewed to understand design procedures and obtain design constraints and parameters. The design of the prototype that included flywheel, clutch, CVT and large vehicle inertia in series was implemented in the computer software CATIA. Materials were procured to fabricate the components, and these components were assembled. Then the hardware of a control system was integrated into the assembled system. The prototyping of the flywheel system was completed with the budget of $10,942.8. Basic experiments were conducted using the flywheel prototype to characterize the speed profiles of the flywheel and vehicle inertias. An energy analysis of the energy transfer process at each stage is studied to estimate the dissipation of energy in the designed prototype. The two-way efficiency for kinetic energy transfer processes is about 20.0% for the prototype. Accounting for the significant friction and aerodynamic drag force that always exist in the experiment at each stage, the overall efficiency of the prototype is about 1.6%.

The flywheel system prototype built as part of this work lends itself to further modeling, analysis, and control studies. First, more advanced control strategies can be developed to optimize the control systems. Then more experiments could be conducted to improve model accuracy. Finally, the energy losses associated with various components of the energy storage system can be analyzed.

BIBLIOGRAPHY

[1] Oil Consumption in North America. http://maps.unomaha.edu/peterson/funda/sidebar/oilconsumption.html.

[2] Retail Price Chart. http://www.columbusgasprices.com/Retail_Price_Chart.aspx.

[3] Energy flow charts from Lawrence Livermoore National Laboratories. https://flowcharts.llnl.gov/.

[4] McDonough, J. *System Dynamics Modeling and Development of a Design Procedure for Short-term Alternative Energy Storage Systems*, M.S. Thesis, The Ohio State University, 2011.

[5] Cumulative worldwide sales of Toyota hybrids top 3M units. http://www.greencarcongress.com/2011/03/cumulative-worldwide-sales-of-toyota-hybrids-top-3m-units.html.

[6] Guzzella, L., Sciarretta, A. *Vehicle Propulsion Systems Introduction to Modeling and Optimization* (2nd ed.). Springer: New York.

[7] Barr, A., Veshagh, A. *Fuel Economy and Performance Comparison of Alternative Mechanical Hybrid Powertrain Configurations*. SAE 2008 International. Number 2008-01-0083.

[8] Brockbank, C., Greenwood, C. *Fuel Economy Benefits of a Flywheel & CVT Based Mechanical Hybrid for City Bus and Commercial Vehicle Applications*. SAE 2009 International. Number 2009-01-2868.

[9] Flybrid Systems.

http://www.flybridsystems.com/F1System.html.

[10] Canova, M., Bolletta, A., Chiara, F., McDonough, J. et al., "*A Design Procedure for Alternative Energy Storage Systems for Hybrid Vehicles*," SAE Technical Paper 2011-24-0079, 2011.

[11] McDonough, J., Jebakumar, K., Chiara, F., Canova, M. *Energy-based Modeling of Alternative Energy Storage Systems for Hybrid Vehicles*. DSCC 2011.

[12] Collins, J., Busby, H., Staab, G. *Mechanical Design of Machine Elements and Machines*. John Wiley & Sons, Inc. ISBN 978047041303-6.

[13] L600 Friction Clutch Product Details from Nexen Group.

http://www.nexengroup.com/default/products/details/id/805283.

[14] KOPP Variable Speed Drive Brochure.

http://www.allspeeds.co.uk/wp-content/files_mf/brochure.pdf.

[15] Control Air Inc, Electro Pneumatic Valve Manual.

http://www.dwn.ie/pdf/control_air/500_spec.pdf.

[16] Shielded Inductive Sensors Manual.

http://www.omega.com/Pressure/pdf/PRX102.pdf.

[17] Jebakumar, Kingsly. *Modeling, Control and Prototyping of Alternative Energy Storage Systems for Hybrid Vehicles*. M.S. Thesis. The Ohio State University, 2012.